

**EFFECTS OF WATER ON THE METHANE HYDRATE FORMATION  
AND DISSOCIATION WITH HOLLOW SILICA AND ACTIVATED  
CARBON**

Sarocha Rungrussamee

A Thesis Submitted in Partial Fulfilment of the Requirements  
for the Degree of Master of Science  
The Petroleum and Petrochemical College, Chulalongkorn University  
in Academic Partnership with  
The University of Michigan, The University of Oklahoma,  
Case Western Reserve University, and Institut Français du Pétrole  
2018

บทคัดย่อและแฟ้มข้อมูลฉบับเต็มของวิทยานิพนธ์ตั้งแต่ปีการศึกษา 2554 ที่ให้บริการในคลังปัญญาจุฬาฯ (CUIR)  
เป็นแฟ้มข้อมูลของนิสิตเจ้าของวิทยานิพนธ์ที่ส่งผ่านทางบัณฑิตวิทยาลัย

The abstract and full text of theses from the academic year 2011 in Chulalongkorn University Intellectual Repository (CUIR)  
are the thesis authors' files submitted through the Graduate School.

**Thesis Title:** Effects of Water on the Methane Hydrate Formation and  
Dissociation with Hollow Silica and Activated Carbon  
**By:** Sarocha Rungrussamee  
**Program:** Petroleum Technology  
**Thesis Advisors:** Prof. Pramoch Rangsunvigit  
Dr. Santi Kulprathipanja

---

Accepted by The Petroleum and Petrochemical College, Chulalongkorn  
University, in partial fulfilment of the requirements for the Degree of Master of  
Science.

..... College Dean  
(Prof. Suwabun Chirachanchai)

**Thesis Committee:**

.....  
(Prof. Pramoch Rangsunvigit)

.....  
(Dr. Santi Kulprathipanja)

.....  
(Assoc. Prof. Boonyarach Kitiyanan)

.....  
(Dr. Tanate Danuthai)

**ABSTRACT**

5973013063: Petroleum Technology

Sarocho Rungrussamee: Effects of Water on the Methane Hydrate Formation and Dissociation with Hollow Silica and Activated Carbon

Thesis Advisors: Prof. Pramoch Rangsunvigit, Dr. Santi Kulprathipanja 71 pp.

Keywords: Methane hydrate/ Hollow silica/ Activated carbon/ Water ratio

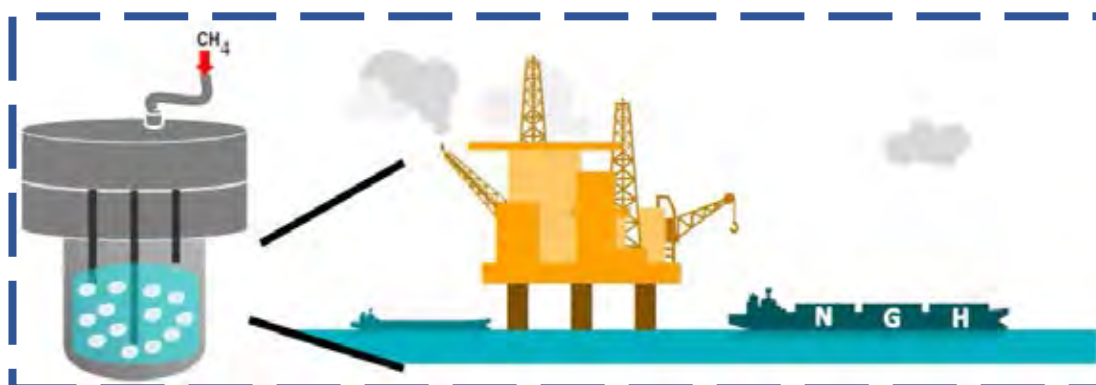
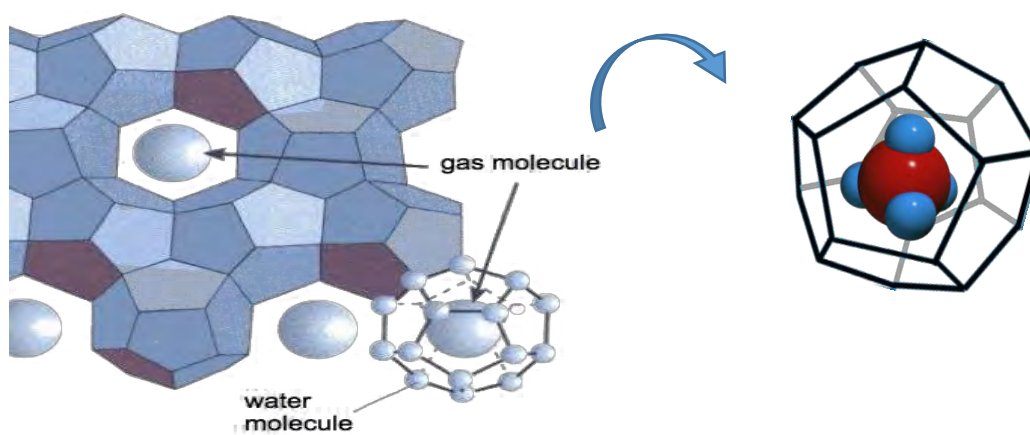
The porous materials, hollow silica (HSC) and activated carbon (AC), were selected to investigate their effects with water on methane hydrate formation and dissociation. The methane hydrate formation with the porous materials was conducted at 8 MPa and 277 K. The dissociation of hydrates was achieved by thermal stimulation with 294 K temperature driving force. The result showed that the hydrate formation of the system with 1:14 HSC to water ratio, the system with excess water, provided the highest methane consumed and water conversion to hydrates. That is because the HSC has low density allowing it to float on water and small particle size leading to the highest volume of water in the system. However, the excess water increased the mass transfer resistance obstructing the gas to dissolve into the water. The system with 1:0.8 AC to water ratio, water deficit, had the lowest methane consumed and water conversion to hydrates. That is because its hydrophilic nature and capillary effect caused by AC small pores. This resulted in the insufficient water to convert to hydrates and led to the low methane consumed. However, the AC has a large surface area and can adsorb methane. And that may aid the gas solubility and fast induction time of the system with the AC. The final methane recovery was about the same in the systems with the HSC and AC at the same temperature driving force (294 K). Therefore, the amount of water and type of porous materials could play important roles on the methane hydrate formation.

## บทคัดย่อ

สโรชา รุ่งรัศมี : ผลของการใช้น้ำบนซิลิกาแบบกลวงและถ่านกัมมันต์ในการเกิดและการสลายตัวของมีเทนไฮเดรต (Effects of Water on the Methane Hydrate Formation and Dissociation with Hollow Silica and Activated Carbon) อ. ที่ปรึกษา : ศ. ดร. ปราโมช รังสรรค์วิจิตร และ ดร. สันติ กุลประทีปปัญญา 71 หน้า

งานวิจัยนี้ศึกษาผลของวัสดุที่มีรูพรุน ได้แก่ ซิลิกาแบบกลวง (hollow silica) และ ถ่านกัมมันต์ (activated carbon) และสัดส่วนของวัสดุที่มีรูพรุนต่อปริมาณน้ำต่อการเกิดและการสลายตัวของมีเทนไฮเดรต (methane hydrate) เนื่องจากซิลิกาแบบกลวงและถ่านกัมมันต์มีพื้นที่ผิว และมีความเป็นรูพรุนสูง ในการศึกษาได้แปรเปลี่ยนสัดส่วนน้ำต่อปริมาณวัสดุรูพรุนด้วยระดับน้ำต่ำกว่าระดับของวัสดุ ระดับน้ำเท่ากับระดับวัสดุ และระดับน้ำสูงกว่าวัสดุ ที่ความดัน 8 MPa และ 277 K ส่วนการสลายตัวของมีเทนไฮเดรตดำเนินโดยวิธีการกระตุ้นด้วยความร้อน (thermal stimulation) ที่อุณหภูมิขับเคลื่อน (driving force) 294 K ผลการทดลองแสดงให้เห็นว่ารูปแบบของวัสดุที่มีรูพรุนกับระดับน้ำต่างๆ ในการเกิดของมีเทนไฮเดรตแตกต่างกัน ยังพบว่าเปอร์เซ็นต์การกักเก็บมีเทนและการเปลี่ยนแปลงของน้ำเป็นไฮเดรตที่ระดับของน้ำสูงกว่าระดับของวัสดุซิลิกาแบบกลวงนั้นสูงที่สุด และระยะเวลาที่ใช้ในการเกิดไฮเดรตครั้งแรกของระบบที่ใช้ระดับน้ำต่ำกว่าระดับของวัสดุถ่านกัมมันต์นั้นเร็วที่สุด ขณะเดียวกันพบความแตกต่างของวัสดุที่มีรูพรุนต่อระดับน้ำไม่มีผลต่อการสลายตัวของมีเทนไฮเดรต ดังนั้นซิลิกาแบบกลวงเป็นวัสดุที่มีรูพรุนที่มีประสิทธิภาพในการกักเก็บมีเทนและเปลี่ยนน้ำไปเป็นไฮเดรตในระบบของระดับน้ำสูงกว่าระดับของวัสดุ และถ่านกัมมันต์เป็นวัสดุที่มีรูพรุนที่ช่วยให้เกิดไฮเดรตได้เร็วในระบบของระดับน้ำต่ำกว่าระดับของวัสดุ

## GRAPHICAL ABSTRACT



● Porous materials: Hollow silica, Activated carbon

Hydrate Formation: 8 MPa and 277 K

Hydrate Dissociation: Temperature driving force 21 °C

## ACKNOWLEDGEMENTS

I would first like to take this opportunity to expose my sincere appreciation to my advisor, Prof. Pramoch Rangsunvigit, for the consistent help of my Master's Degree and related research. His supervision helped me to direct the right research and writing this thesis.

I would also like to thank my co-advisor, Dr. Santi Kulprathipanja, for his helpful suggestion and immense knowledge, which was very helpful to grab new ideas.

My sincere thanks also goes to Assoc. Prof. Boonyarach Kitiyanan and Dr. Tanate Danuthai who were involved in the validation survey for this research project.

I am grateful for the partial scholarship and partial funding of the thesis work provided by the Petroleum and Petrochemical College.

This thesis work is funded by The 90<sup>th</sup> Anniversary of Chulalongkorn University Fund and Grant for International Integration: Chula Research Scholar, Ratchadaphiseksomphot Endowment Fund, Chulalongkorn University, Thailand; The Petroleum and Petrochemical College; and the Center of Excellence on Petrochemicals, and Materials Technology, Thailand.

I would like to thank the entire faculty and staff at The Petroleum and Petrochemical College, Chulalongkorn University for their kind assistance and cooperation.

Finally, I must express my very profound gratitude to my parents and to my friends for providing me with unfailing support and continuous encouragement throughout my years of study and through the process of researching and writing this thesis. This accomplishment would not have been possible without them. Thank you.

## TABLE OF CONTENTS

	<b>PAGE</b>
Title Page	i
Abstract (in English)	iii
Abstract (in Thai)	iv
Graphical Abstract	v
Acknowledgements	vi
Table of Contents	vii
List of Tables	x
List of Figures	x
<b>CHAPTER</b>	
<b>I INTRODUCTION</b>	<b>1</b>
<b>II THEORETICAL BACKGROUND AND LITERATURE REVIEW</b>	<b>3</b>
2.1 Natural Gas	3
2.2 Natural Gas Storage	4
2.2.1 Compressed Natural Gas (CNG)	4
2.2.2 Liquefied Natural Gas (LNG)	5
2.2.3 Adsorbed Natural Gas (ANG)	5
2.2.4 Solidified Natural Gas (SNG)	5
2.3 Gas Hydrates	6
2.3.1 Structures of Gas Hydrates	6
2.3.2 Physical Properties	8
2.3.3 Methane Hydrate in Natural Resource	10
2.3.4 Gas Hydrate Formation	12
2.3.5 Gas Hydrates Dissociation	13
2.4 Literature Reviews	14

<b>CHAPTER</b>	<b>PAGE</b>
<b>III EXPERIMENTAL</b>	<b>30</b>
3.1 Materials and Equipments	30
3.1.1 Materials	30
3.1.2 Equipments	30
3.2 Experimental Procedures	30
3.2.1 Experimental Apparatus	30
3.2.2 Methane Hydrate Formation	31
3.2.3 Methane Hydrate Dissociation	32
<b>IV RESULTS AND DISCUSSION</b>	<b>34</b>
4.1 Effects of Hollow Silica	34
4.1.1 Methane Hydrate Formation	34
4.1.2 Methane Hydrate Dissociation	41
4.2 Effects of Activated Carbon	44
4.2.1 Methane Hydrate Formation	44
4.2.2 Methane Hydrate Dissociation	50
4.3 Comparison between the Effects of Hollow Silica and Activated Carbon to Water Ratio	54
<b>V CONCLUSIONS AND RECOMMENDATIONS</b>	<b>58</b>
<b>REFERENCES</b>	<b>60</b>
<b>APPENDICES</b>	<b>64</b>
<b>Appendix A</b> Calculation for the Methane Consumption	64
<b>Appendix B</b> Calculation for the Conversion of Water to Hydrate	67
<b>Appendix C</b> Calculation for the Percentage of Methane Recovery	68



	<b>PAGE</b>
<b>Appendix D Reused Hollow Silica</b>	69
<b>CURRICULUM VITAE</b>	71

**LIST OF TABLES**

<b>TABLE</b>		<b>PAGE</b>
2.1	Properties of different hydrate structures	8
2.2	Comparison of properties of ice, sI, and sII hydrate crystal structures	9
2.3	Summary of experimental conditions and results of methane hydrate formation in porous media	15
2.4	Experimental results of methane storage in hydrates	17
2.5	Hydrate Formation Experiments Conducted at 277.2 K	19
2.6	The experimental conditions and results	22
4.1	Methane hydrate formation experimental conditions with the presence of hollow silica at 8 MPa and 277 K	36
4.2	Methane hydrate dissociation experimental conditions in the system with the presence of hollow silica using $^a\Delta T = 294$ K	42
4.3	Methane hydrate formation experimental conditions in the system with the presence of activated carbon at 8 MPa and 277 K	46
4.4	Methane hydrate dissociation experimental conditions in the system with activated carbon at difference water ratio with driving force 294 K	52
S1	Methane hydrate formation experimental conditions in the system with the presence of hollow silica	70

## LIST OF FIGURES

FIGURE	PAGE
2.1	Petroleum and natural gas formation. 3
2.2	Gas transport options. 4
2.3	Methane hydrates on fire ice. 6
2.4	Structure types of gas hydrates. 7
2.5	Location of sampled and inferred gas hydrate occurrences worldwide. 10
2.6	Methane hydrate deposit models. 11
2.7	Global inventory of methane hydrate deposits. 11
2.8	Methane hydrate stability chart. 13
2.9	Comparison of methane gas uptake curves between water system (W1-W3), NaCl 1.5 wt% (D1-D3) and NaCl 3.0 wt% (C1-C3) conducted at 8 MPa. 15
2.10	Methane release curve from hydrates formed in water, 1.5 wt% NaCl and 3.0 wt% NaCl. 16
2.11	Effects of different surfactants on methane hydrate formation (1) $300 \times 10^{-6}$ SDS, (2) $500 \times 10^{-6}$ APG; Reaction conditions: $p = 4.34$ MPa, $T = 274.05$ K. 17
2.12	Gas hydrate yield at different initial pressure in methane-water-silica systems. 18
2.13	Comparison of gas uptakes of pure water and seawater experiments at 8 MPa and 277.2 K. 19
2.14	Comparison of the average rate of hydrate formation between seawater and pure water experiments. 20
2.15	Comparison of the number of gas moles recovered from hydrates of seawater and pure water at 4.8 MPa. 21

<b>FIGURE</b>	<b>PAGE</b>
2.16 Gas uptake curves of the hydrate formation in silica gels with the various particle diameter ranges at the bath temperature of 276.15 K and the initial pressure of 9.4 MPa.	23
2.17 Gas uptake curves of the hydrate formation in silica gels with various pore diameters and the particle diameter range of 0.105-0.150 mm at the temperature of 276.15 K and the initial pressure of 9.4 MPa.	24
2.18 Comparison of the rate of methane release and methane recovery from the hydrate dissociation experiment carried out at 8 MPa and $\Delta T=294$ K.	25
2.19 Comparison of the average hydrate growth during the methane hydrate formation at 8 MPa and 277 K with the activated carbon particle sizes of 250– 420 $\mu\text{m}$ , 420– 841 $\mu\text{m}$ , and 841–1680 $\mu\text{m}$ .	25
2.20 Enhanced methane uptake by adding THF as a promoter in a UTR.	27
2.21 Percentage of water to hydrate conversion for all of the formation experiments conducted at 277 K and three different bed sizes. Time zero represents the nucleation point. Blue color lines represent the experiments for the largest bed size (CR). Black color lines represent the experiments for the medium bed size (CR + CC1). Red color lines represent the experiments for the smallest bed size (CR + CC1 + CC2).	28
3.1 Schematic diagram of gas hydrate apparatus; a) schematic diagram, b) cross-section of a crystallizer.	31

<b>FIGURE</b>	<b>PAGE</b>
4.1 Gas uptake and temperature profiles during the methane hydrate formation of the HSC/H <sub>2</sub> O/CH <sub>4</sub> system at 8 MPa and 277 K and 1:10 HSC to water ratio (Experiment 3, Table 4.1).	37
4.2 Gas uptake and temperature profiles during the methane hydrate formation of the HSC/H <sub>2</sub> O/CH <sub>4</sub> system at 8 MPa and 277 K and 1:12 HSC to water ratio (Experiment 5, Table 4.1).	37
4.3 Gas uptake and temperature profiles during the methane hydrate formation of the HSC/H <sub>2</sub> O/CH <sub>4</sub> system at 8 MPa and 277 K and 1:14 HSC to water ratio (Experiment 9, Table 4.1).	38
4.4 Morphology of hollow silica by scanning electron microscope (SEM) (a) Particle of hollow silica in different sizes, (b) Breakage hollow silica.	39
4.5 Comparison of hydrate growth during the methane hydrate formation in the system of HSC/H <sub>2</sub> O/CH <sub>4</sub> at 8 MPa and 277 K and various HSC to water ratios (1:10, 1:12, and 1:14). Time zero in the figure corresponds to the first point of hydrate growth.	40
4.6 Methane released and temperature profiles in the system of the HSC/H <sub>2</sub> O/CH <sub>4</sub> with the 1:10 HSC to water ratio and temperature driving force = 294 K (Experiment 12, Table 4.2).	43
4.7 Methane released and temperature profiles in the system of HSC/H <sub>2</sub> O/CH <sub>4</sub> with the 1:12 HSC to water ratio and temperature driving force = 294 K (Experiment 14, Table 4.2).	43

<b>FIGURE</b>		<b>PAGE</b>
4.8	Methane released and temperature profiles in the system of HSC/H <sub>2</sub> O/CH <sub>4</sub> with the 1:14 HSC to water ratio and temperature driving force = 294 K (Experiment 18, Table 4.2).	44
4.9	Gas uptake and temperature profiles during the methane hydrate formation of AC/H <sub>2</sub> O/CH <sub>4</sub> system at 8 MPa and 277 K and 1:0.8 AC to water ratio (Experiment 20, Table 4.3).	47
4.10	Gas uptake and temperature profiles during the methane hydrate formation of AC/H <sub>2</sub> O/CH <sub>4</sub> system at 8 MPa and 277 K and 1:1 AC to water ratio (Experiment 22, Table 4.3).	57
4.11	Gas uptake and temperature profiles during the methane hydrate formation of AC/H <sub>2</sub> O/CH <sub>4</sub> system at 8 MPa and 277 K and 1:1.2 AC to water ratio (Experiment 27, Table 4.3).	48
4.12	Comparison of hydrate growth during the methane hydrate formation in the system of AC/H <sub>2</sub> O/CH <sub>4</sub> at 8 MPa, 277 K, 1:0.8, 1:1, and 1:1.2 AC to water ratio (Experiments 20, 22, and 27 respectively, Table 4.3). Time zero in the figure corresponds to the first point of hydrate growth.	50
4.13	Methane released and temperature profiles in the system of AC/H <sub>2</sub> O/CH <sub>4</sub> at 1:0.8 AC to water ratio and temperature driving force = 294 K (Experiment 29, Table 4.4).	53
4.14	Methane released and temperature profiles in the system of AC/H <sub>2</sub> O/CH <sub>4</sub> at 1:1 AC to water ratio and temperature driving force = 294 K (Experiment 31, Table 4.4).	53
4.15	Methane released and temperature profiles in the system of AC/H <sub>2</sub> O/CH <sub>4</sub> at 1:1.2 AC to water ratio and temperature driving force = 294 K (Experiment 36, Table 4.4).	54

<b>FIGURE</b>		<b>PAGE</b>
4.16	Comparison of gas uptake during the methane hydrate formation in the system of water deficit (1:10 HSC to water ratio and 1:0.8 AC to water ratio) with the present of HSC and AC at 8 MPa and 277 K.	56
4.17	Comparison of gas uptake during the methane hydrate formation in the system of water saturated (1:12 HSC to water ratio and 1:1 AC to water ratio) with the present of HSC and AC at 8 MPa and 277 K.	57
4.18	Comparison of gas uptake during the methane hydrate formation in the system of excess water (1:14 HSC to water ratio and 1:1.2 AC to water ratio) with the present of HSC and AC at 8 MPa and 277 K.	57
S1	Gas uptake and temperature profiles during the methane hydrate formation of the HSC/H <sub>2</sub> O/CH <sub>4</sub> system at 8 MPa and 277 K (Fresh HSC).	69
S2	Gas uptake and temperature profiles during the methane hydrate formation of the HSC/H <sub>2</sub> O/CH <sub>4</sub> system at 8 MPa and 277 K (Reused HSC).	69

## CHAPTER I

### INTRODUCTION

Natural gas has received much attention as alternative energy with clean burning and low CO<sub>2</sub> emission. The main component of natural gas is methane, whose boiling point is -162 °C under 0.1 MPa. There are three main options for natural gas storage, CNG (Compressed Natural Gas), LNG (Liquefied Natural Gas), and ANG (Adsorbed Natural Gas). For CNG, natural gas is stored at a high pressure, preventing storage in a large scale. For LNG, there is a problem of boil-off gas (BOG), which changes the quantity of LNG over time. For ANG via sorbents, natural gas is adsorbed onto sorbents including activated carbon, graphene, metal organic frameworks (MOFs) etc. In order to accommodate natural gas as a large scale, the new technology to store and transport natural gas is SNG (Solidified Natural Gas), which is operated at high pressure and low temperature. Furthermore, it can be safer and more economical than that of traditional methods (Veluswamy *et al.*, 2016).

Natural gas hydrates are crystalline, ice-like solid composed of gas molecules (guest molecule) trapped with cages formed by water molecules. SNG presents the best option to store natural gas in a large scale with high volumetric storage capacity, 1 m<sup>3</sup> of methane hydrates contains 170 m<sup>3</sup> of methane gas at STP (Englezos and Lee, 2005), not sensitive to the presence of trace hydrocarbon, environmentally friendly, no toxic emission, and non-eruption nature, extremely safe and cost effective (Javanmardi *et al.*, 2005). Natural gas hydrates have attracted much heed as a new means for store and transport natural gas. However, the applications of hydrate storage have been hindered by some problems, for instant, slow kinetics of hydrate formation, interstitial water unreacted, economy of scale up, and the reliability of hydrate storage capacity. Adding promoters can solve that problems by using thermodynamic promoters and kinetic promoters to accelerate the hydrate formation conditions providing one of the flexible and easiest ways to increase the rate of hydrate formation (Sloan and Koh, 2007).

In the laboratory, where stirred tank reactors are employed, once the hydrates form, the water conversion to hydrates is low because of the agglomeration of hydrate crystals at the interface (Seo *et al.*, 2014). Effects of additives such as SDS (sodium



dodecyl sulfate), APG (alkyl polysaccharide glycoside), and CP (liquid hydrocarbon cyclopentane) were investigated. SDS was reported to be one of the best additives that can reduce the hydrate induction time, improved hydrate formation rate and storage gas capacity (Sun *et al.*, 2004). Effects of particle size of porous media like activated carbon were also investigated. The experiment with 250 to 420  $\mu\text{m}$  activated carbon showed the fastest methane consumption and methane recovery due to the small particle size had high interconnectivity, which increased the contact area between gas and water, while the large particle size from 841 to 1680  $\mu\text{m}$  stored the highest methane because it had a large interstitial space and high conversion of water to hydrate (Siangsai *et al.*, 2015). Maize starch was also investigated as a porous media to enhance methane hydrate formation with different concentrations of maize starch on methane hydrate formation and dissociation. It was reported that the high concentration, 800 ppm, increased the formation rate up to 2.5 times compared with no maize starch (Babakhani and Alamdari, 2015). Hollow silica is another porous material with increased attention. Prasad *et al.* (2014) used hollow silica to enhance methane storage capacity in the gas hydrates. They concluded that the hollow silica structure contained an inner void surrounded by a thinner solid shell. Thus, it could improve the hydrate formation kinetics at a high pressure and low temperature and extremely fast hydrate conversion.

The effects of promoters and porous material to water ratios were mostly, if not all, reported using a stirred reactor. Few reported these effects on an unstirred reactor. Thus, the purpose of this work was to study effects of different porous materials including hollow silica and activated carbon and the amount of water on porous material to water ratio on the hydrate formation/dissociation in an unstirred reactor.

## CHAPTER II

### THEORETICAL BACKGROUND AND LITERATURE REVIEW

#### 2.1 Natural Gas

Natural gas is a mixture hydrocarbon gas consisting of mainly methane and it can include various amounts of other higher alkanes, and a small percentage of carbon dioxide, nitrogen, hydrogen sulfide, or helium. It is formed by breaking down of animals and plants deposit under the surface of the Earth, sometimes mixed with sand and silt. Over time, these layers were buried under sand, silt, and rock, at intense heat and pressure over thousands of years and that condition can changed some of organic materials to oil, coal, and natural gas. Natural gas is colorless, shapeless, and odorless gas ([www.socratic.org](http://www.socratic.org)).

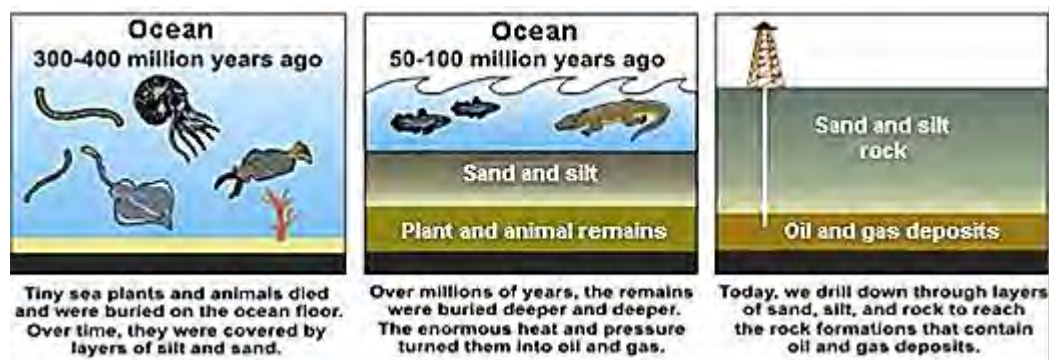


**Figure 2.1** Petroleum and natural gas formation ([www.socratic.org](http://www.socratic.org)).

Natural gas is non-renewable energy that is often used for heating, cooking, power generation and fuel in vehicles. When it is burned, it will give a lower level of emission. That is to say, natural gas is one of the cleanest burning fossil fuel ([www.naturalgas.org](http://www.naturalgas.org)).

The major issues in the use of natural gas is transportation and storage because of its low density ([www.ucsusa.org](http://www.ucsusa.org)). Normally, natural gas can be stored in storage tank or underground and it can be transported by ship, pipe, or truck.

## 2.2 Natural Gas Storage

In recent year, natural gas has gained much attention in terms of green alternative energy but gas is difficult to store or transport because of its physical nature and needs high pressures and/or low temperatures to increase the bulk density (Thomas and Dawe, 2003). Figure 2.2 shows a number of methods of exporting gas energy. Methods include pipelines, liquefied natural gas (LNG), gas to liquids (GtL), gas to commodity (GtC), gas to wire (GtW), for instance, generate electricity at the producing field and transport the electricity by cable, compressed natural gas (CNG), and gas to solids (GtS), such as hydrates.

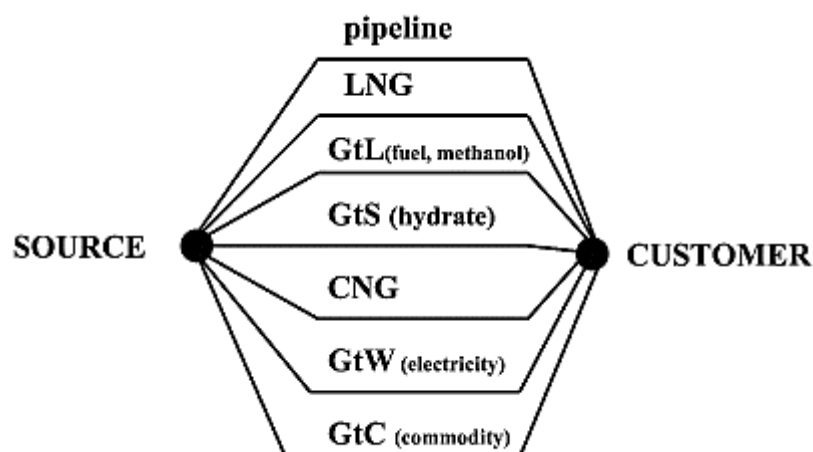


**Figure 2.2** Gas transport options (Thomas and Dawe, 2003).

The choice of these technologies depends on many factors such as the scale of development and distance from markets. Thus, natural gas storage facilities are essential for storing excess gas to use when demand increasing. There are four major methods to store gas (Thomas and Dawe, 2003).

### 2.2.1 Compressed Natural Gas (CNG)

Compressed natural gas is stored in the condition of high pressure container 20 to 25 MPa (200 to 250 bar, or 3,000 to 3,600 psi). CNG also contains

hydrocarbons like ethane, propane, and other gases like carbon dioxide, nitrogen, helium, and sulphur compounds (a sulphur odor is added to CNG for leak detection). CNG is an economic solution for long distant offshore gas with small and medium reserves. It is usually used in a small fueling location and on vehicle. However, CNG requires greater space for gas storage in the same amount of gas compared to others technologies ([www.afsglobal.com](http://www.afsglobal.com)).

### 2.2.2 Liquefied Natural Gas (LNG)

Liquefied natural gas is stored as super cooled liquid or cryogenic at temperature that can condense natural gas to liquid, which relies on composition of gas, and temperature is between -120 and -170 °C ([www.afsglobal.com](http://www.afsglobal.com)). LNG can decrease costs for port facilities, and it offers an energy density similar to diesel fuels. However, the disadvantage of LNG is high cost of cryogenic storage and, in some cases, Boil-Off Gas (BOG), which is the problem to storage and changes the quality of LNG over time ([www.fluenta.com](http://www.fluenta.com)).

### 2.2.3 Adsorbed Natural Gas (ANG)

Adsorbed natural gas stores natural gas in various sponge like materials, such as activated carbon, carbon nanotubes, graphene, and MOFs (metal-organic frameworks) with standard pressure and temperature. An increase or decrease of pressure or temperature affects adsorption and desorption process. ANG has never been commercialized because of its technical drawbacks. For instant, the storage capacity is low compared to CNG and LNG (Asheh and Emadi, 2008).

### 2.2.4 Solidified Natural Gas (SNG)

SNG can store natural gas via clathrate hydrates. This method occurs under high pressure and low temperature, which offers an excellent storage on a large scale. It turns natural gas into hydrates by trapping gas molecules with water molecules. Hydrates are increasingly interesting as a storage method for natural gas because of its advantages: easy to storage, economy of scale up, simple transportation, and effective recovering of the natural gas from this storage (Veluswamy *et al.*, 2016).

## 2.3 Gas Hydrates

Gas hydrates (or clathrate hydrates) are ice-like crystalline solid, where gas (guest molecule) is surrounded by water cage molecules (host molecule) at feasible formation condition. In the past, gas hydrates are problems of off-shore exploration and production as the gas plugging in pipelines. However, gas hydrates become more interesting due to a huge reservoirs of methane hydrates were discovered, and its technology can be used at a large scale to store gas for the ease of transportation. Clathrate hydrates are stable under moderate pressure (typically of a few MPa) and very low temperature typically close to 273 K. Methane hydrate samples are easily burnt in the barometric pressure. Figure 2.3 shows the methane hydrates were ignited in ice form – hence the “fire ice” moniker ([www.theenergycollective.com](http://www.theenergycollective.com)). When methane hydrates were either warmed or depressurized, they were called dissociation. The crystalline lattices were broken down into liquid water and released gas.



**Figure 2.3** Methane hydrates on fire ice ([www.theenergycollective.com](http://www.theenergycollective.com)).

### 2.3.1 Structures of Gas Hydrates

Gas hydrates are composed of three main clathrate repeating crystal structures: I, II and H. The type of hydrates that forms depends mainly on the molecular diameters of the gas molecules included in the hydrates. (Ballard and Sloan, 2000).

1. The structure I or sI, a body-centered cubic structure, gas hydrates can hold small gas molecules (0.4–0.55 nm), forms with natural gases containing molecules smaller than propane; accordingly, sI hydrates are found in situ in deep oceans with biogenic gases containing mostly methane, carbon dioxide, and hydrogen sulfide.

2. The structure II or sII, a diamond lattice within a cubic framework, gas hydrates can maintain relatively large molecules (0.6–0.7 nm), forms when natural gases or oils contain molecules larger than ethane but smaller than pentane; sII represents hydrates from thermogenic gases

3. The structure H or sH gas hydrates can only contain mixture of large and small molecules (0.8-0.9 nm) such as methyl cyclohexane and methane. Structure H hydrates require a small occupant (like methane, nitrogen, or carbon dioxide) for the  $5^{12}$  and  $4^35^66^3$  cages but the molecules in the  $5^{12}6^8$  cage can be as large as 0.9 nm (e.g. ethylcyclohexane) (Henriet and Mienert, 1998; Sloan, 1997).

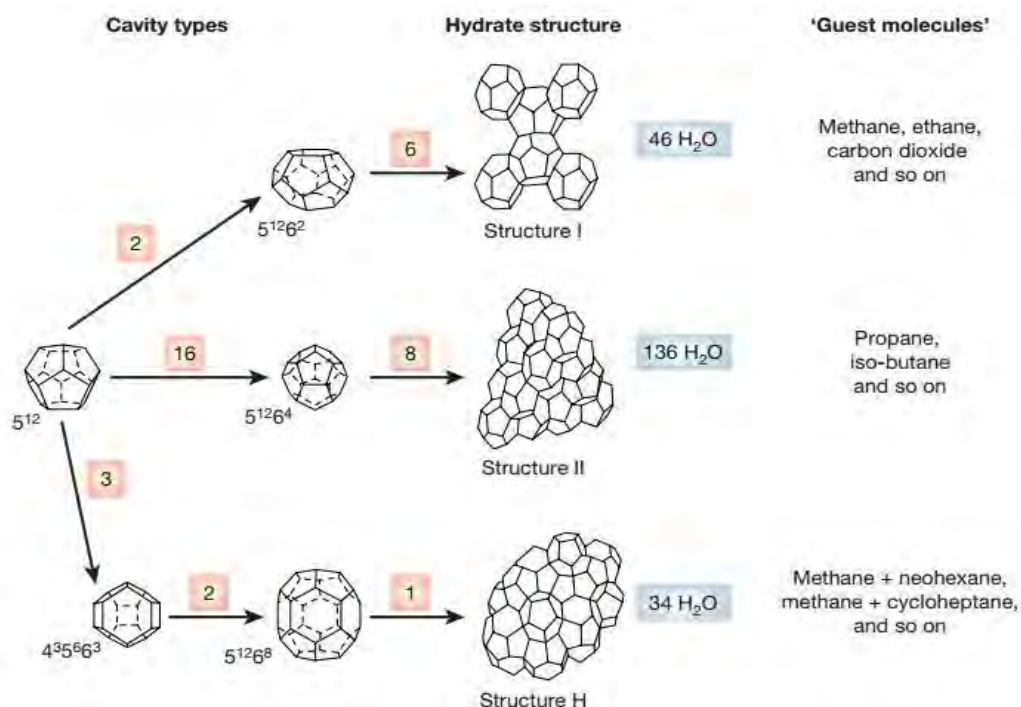


**Figure 2.4** Structure types of gas hydrates (Sloan, 2003).

Figure 2.4 shows the three main common structure types, cavity types, and guest molecules. The symbol  $5^{12}6^4$  specifies a water cage composed of twelve pentagonal and four hexagonal faces. The number in squares means the number of cage types. For example, the structure I unit crystal is composed of 46 water molecules per 8 gas molecules consisting of 2 small and 6 large cages. And the properties of different hydrate structures as in Table 2.1.

**Table 2.1** Properties of different hydrate structures (Sloan, 1997)

cavity	I		II		H		
	small	large	small	large	small	medium	large
description	$5^{12}$	$5^{12}6^2$	$5^{12}$	$5^{12}6^4$	$5^{12}$	$4^35^66^3$	$5^{12}6^8$
no. of cavities/unit cell	2	6	16	8	3	2	1
av cavity radius, Å	3.95	4.33	3.91	4.73	3.91 <sup>c</sup>	4.06 <sup>c</sup>	5.71 <sup>c</sup>
variation in radius, %	3.4	14.4	5.5	1.73	not available		
coordination number <sup>b</sup>	20	24	20	28	20	20	36
no. of waters/unit cell	46		136		34		

<sup>a</sup> Variation in distance of oxygen atoms from center of cage. <sup>b</sup> Number of oxygens at the periphery of each cavity. <sup>c</sup> Estimates of structure H cavities from geometric models.

### 2.3.2 Physical Properties

Water molecules are linked through hydrogen bonding and create cavities (host lattice) that can enclose a large variety of molecules (guests). No chemical bonding takes place between the host water molecules and the enclosed guest molecule (Gabitto and Tsouris, 2009). As stated in the hydrate model, the water molecules form a well-defined crystal lattice (the host lattice) containing cavities, into which small gas molecules (guests) may be adsorbed; under appropriate conditions the adsorption energy may then reduce the free energy of the hydrates sufficiently to make the hydrate phase stable than either pure water or ice (Rodger, 1989). The mechanical properties of the three hydrate structures should be similar to those of ice. The mechanical properties of the three hydrate structures are shown in Table 2.2 with the exception of thermal conductivity and thermal expansivity.

The molecular structures are determined by properties of structure I (sI) and structure II (sII), described by three heuristics: (i) Mechanical properties approximate those of ice, yet each volume of hydrate may contain large volumes of the hydrate-forming species at standard temperature and pressure conditions (STP).

(ii) Phase equilibrium is set by the size ratio of guest molecules within host cages, and three-phase (liquid water-hydrate-vapor; L-W-H-V) equilibrium pressure depends exponentially upon temperature. (iii) Heats of formation are set by the hydrogen-bonded crystals and are reasonably constant within a range of guest sizes (Sloan, 1997).

The physical properties of gas hydrates trapped in sediments are very important in detecting the presence of these compounds, estimating the amount of gas hydrates trapped in the sediments, and developing processes to exploit this resource. (Gabitto and Tsouris, 2009). The phase transition that occurs at higher temperatures causes concern when structures are placed in the vicinity of hydrates.

In laboratory and analytical investigation, the interaction between hydrates and the host sediment at the grain level has been highlighted as hydrates are not restricted to forming in a unique way in the pore space. Methane hydrates have a porous nature. The presence of hydrates, which replaces water in pore space, strongly alters the physical properties of the sediments, in which it occurs. The bulk densities of methane hydrates range from 0.35 to 0.75 kg/L and are inversely correlated with the pore volume, which ranges from 10% to 70% by volume. In present, researchers have had only peripheral interest in hydrate mechanical properties.

**Table 2.2** Comparison of properties of ice, sI, and sII hydrate crystal structures (Gabitto and Tsouris, 2009)

Property	Ice ( $I_h$ )	Structure I	Structure II
Water molecules number	4	46	136
Lattice parameters at 273 K, nm	$a = 0.452, c = 0.736$	1.20	1.73
Dielectric constant at 273 K	94	~58	58
Water diffusion correlation time, $\mu$ s	220	240	25
Water diffusion activation energy, kJ/m	58.1	50	50
Isothermal Young's modulus at 268 K, $10^9$ Pa	9.5	8.4 (est.)	8.2 (est.)
Poisson's ratio	0.33	~0.33	~0.33
Bulk modulus (272 K)	8.8	5.6	NA
Shear modulus (272 K)	3.9	2.4	NA
Compressional velocity ( $V_p$ ), m/s	3870.1	3778.0	3821.8
Shear velocity ( $V_s$ ), m/s	1949	1963.6	2001.1
Velocity ratio (comp./shear)	1.99	1.92	1.91
Linear thermal expn., at 200 K, $K^{-1}$	$56 \cdot 10^{-6}$	$77 \cdot 10^{-6}$	$52 \cdot 10^{-6}$
Adiab. bulk compress. (273 K), $10^{-11}$ Pa	12	14 (est.)	14 (est.)
Heat Capacity, $J \cdot kg^{-1} \cdot K^{-1}$	3800	3300	3600
Thermal conductivity (263 K), $W \cdot m^{-1} \cdot K^{-1}$	2.23	$0.49 \pm 0.02$	$0.51 \pm 0.02$
Refractive index, 638 nm, $-3^\circ C$	1.3082	1.3460	1.350
Density, $kg \cdot m^{-3}$	916	912	940



### 2.3.3 Methane Hydrate in Natural Resource

In natural, hydrates can form in fracture between sediments in some regions and deposits at continental margins and under permafrost where hydrates favorable condition. Figure 2.5 shows the natural settings where methane and water are present, and where pressure and temperature conditions are suitable to form and sustain hydrates.

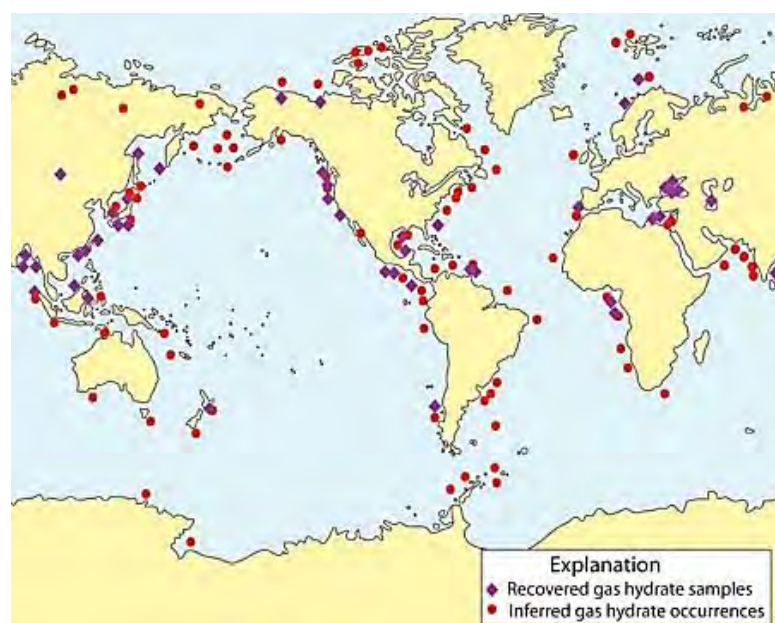


**Figure 2.5** Location of sampled and inferred gas hydrate occurrences worldwide ([www.washingtonpost.com](http://www.washingtonpost.com)).

The environments that have pressure and temperature of methane hydrate favorable, there are four Earth environments: 1) sediment and sedimentary rock units below Arctic permafrost; 2) sedimentary deposits along continental margins; 3) deep water sediments of inland lakes and seas; and 4) under Antarctic ice. With the Antarctic deposits are exception, accumulations of methane hydrates are not much deep below Earth's surface, as shown in Figure 2.6. In most situations, the methane hydrates are within a few hundred meters of the sediment surface ([www.geology.com](http://www.geology.com)).

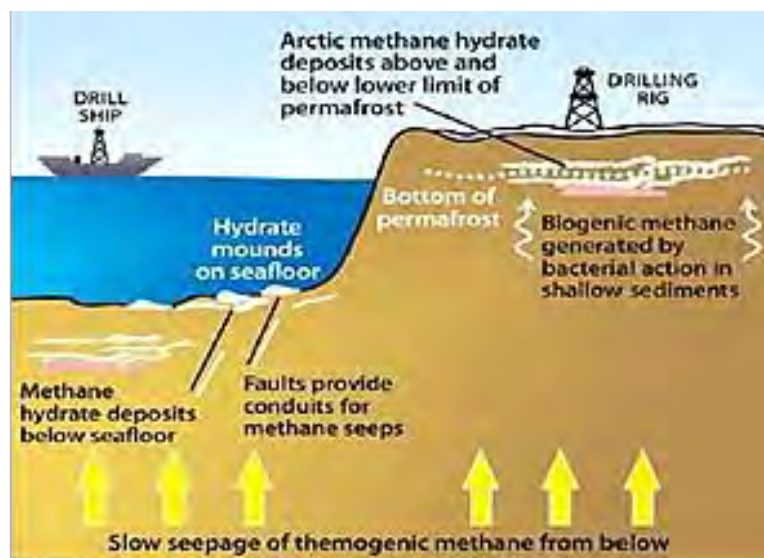


**Figure 2.6** Methane hydrate deposit models ([www.geology.com](http://www.geology.com)).

In these environments, methane hydrates occur in the sediment as layers, nodules, and intergranular cements. The deposits are often so dense and laterally persistent that they produce an impermeable layer that traps natural gas moving upwards from below. Figure 2.7 shows a generalized version of locations in global inventory of natural gas hydrate occurrence database.

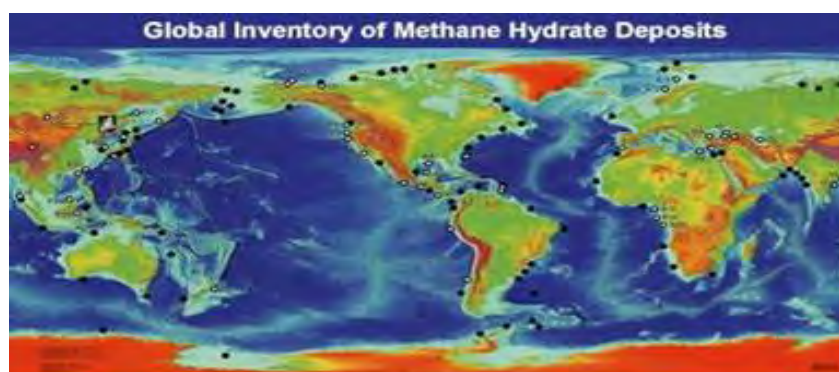


**Figure 2.7** Global inventory of methane hydrate deposits ([www.geology.com](http://www.geology.com)).

#### 2.3.4 Gas Hydrate Formation

Hydrate formation is basically a crystallization process; upon successful hydrate nucleation, a thin hydrate film forms on the water-gas interface, which grows further in a mass transfer limited regime. It has been identified that other than utilizing better reactor designs, higher solubility of hydrate forming guests in water, and a larger contact area between the hydrate formers and water can reduce the mass transfer resistance and ensure faster hydrate growth (Kumar *et al.*, 2015).

The most challenging step of crystallization of gas hydrates is nucleation (dispersion of water and gas clusters that go on until a critically stable sized nucleus has been formed). Furthermore, it could be the key to the kinetic inhibition or promotion of this process. A natural gas hydrate sample of 1 m<sup>3</sup> can produce ~163 m<sup>3</sup> of gas upon dissociation at standard temperature and pressure conditions and hence are considered to be a potential energy source.

Figure 2.8 shows the depth and pressure on the y axis and the temperature on the x axis. The line that separates stability fields of gas, gas hydrates, water and water ice is the dashed lines, and the important line is the line labeled “hydrate to gas transition”. Because the conditions for the formation of methane hydrates occur below this line and above this line the methane hydrate will not form. The line of geotherm specifies the change of temperature with depth at a specific location ([www.geology.com](http://www.geology.com)).

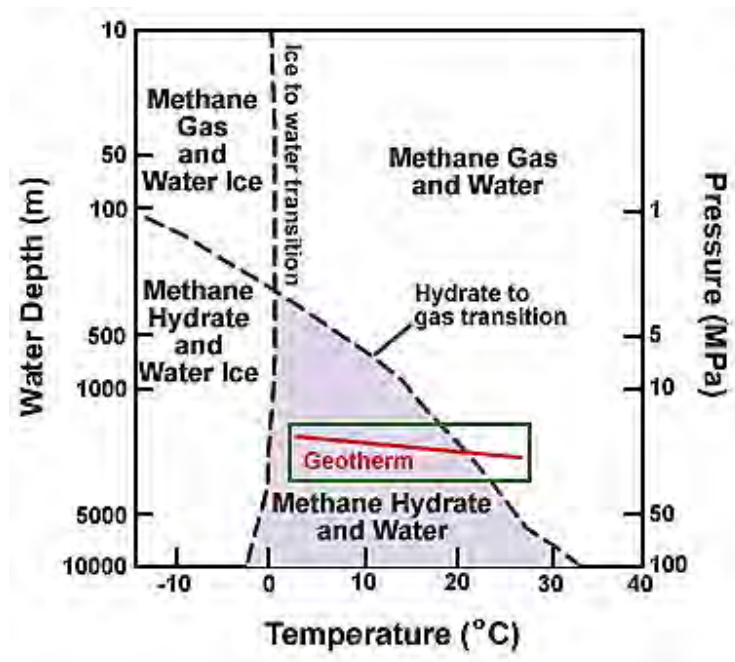


**Figure 2.8** Methane hydrate stability chart (www.geology.com).

### 2.3.5 Gas Hydrates Dissociation

Gas hydrate dissociation is the process, which provides heat to break the hydrogen bonds between water molecules and the van der Waals interaction forces between guest molecule and water molecule of the hydrate lattice. When the process completes, the product of hydrate dissociation is water molecules (host molecules) and gas molecules (guest molecules).

Several conventional methods have been proposed for the production of natural gas from hydrate reservoir, including depressurization, thermal stimulation, chemical inhibitor injection, or a combination of these methods. Depressurization is the most popular method, which includes decreasing the pressure to below the hydrate stability zone. The second method is thermal stimulation, which requires increasing the temperature above the natural gas hydrate equilibrium temperature at the prevailing pressure. The third method is chemical inhibitor injection, which can be differentiated into two different types: thermodynamic inhibitor and kinetic inhibitor injection (Zhenyuan *et al.*, 2016). This method uses some chemical inhibitors to inhibit hydrate formation by using chemical like methanol or glycols and act by shifting the

water/hydrocarbon/ hydrate three-phase equilibrium line. Intrinsic decomposition rate of methane hydrate is controlled by temperature, pressure, interfacial area, and the intrinsic rate constant. It affects the heat transfer rate from surrounding to hydrate core due to the endothermic characteristics of the reaction.

Despite several advantages of solidified natural gas technology, there are hindered by the slow kinetics formation, low hydrate yield, long induction time, and economy of process scale up. So, the main propose of this work was to study factors that affect the hydrate formation rate and storage capacity such as types of porous material and porous material to water ratio.

## **2.4 Literature Reviews**

Chong *et al.* (2015) studied the effect of NaCl on methane hydrate formation and dissociation in porous media in a stirred tank reactor by comparing effects of water (no salt and deionization), 1.5 wt%, and 3.0 wt% NaCl concentration at 8 MPa and 277 K. They found that the presence of NaCl kinetically inhibited hydrate formation due to decreasing of water activity and disturbing to the crystalline structure of hydrates. Therefore, they concluded that NaCl increased the barrier for hydrate nucleation.

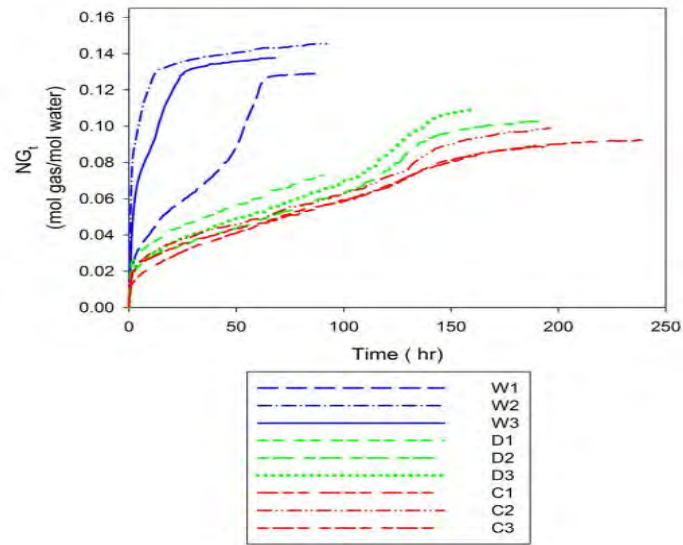


**Figure 2.9** Comparison of methane gas uptake curves between water system (W1-W3), NaCl 1.5 wt% (D1-D3) and NaCl 3.0 wt% (C1-C3) conducted at 8 MPa (Chong *et al.*, 2015).

As an evident from Figure 2.9, the hydrate formation in the 3 and 1.5 wt% salt solution used a longer period of time than in water system. Moreover, there are less consumed gas in salt solution system as shown in Table 2.3.

**Table 2.3** Summary of experimental conditions and results of methane hydrate formation in porous media (Chong *et al.*, 2015)

Exp. No.	NaCl (wt%)	Heating method	Stage 1		$V_{g, 100 \text{ min}}$ ( $\text{m}^3 \text{ gas [STP]} / \text{m}^3 \text{ hydrate}$ )	Recovery (%)
			Rate of $\text{CH}_4$ production [ $R^2$ ] ( $\text{m}^3 \text{ gas [STP]} / \text{m}^3 \text{ hydrate} \cdot \text{min}$ )	% Dissociated		
W1	0	Const.	11.633 [0.9840]	67.32	162.91	97.95
W2	0	Grad.	5.791 [0.9923]	76.77	164.84	99.54
W3	0	Const.	11.043 [0.9911]	67.50	152.59	91.55
Wc	0	Const.	12.260 [0.9629]	74.90	166.66	98.76
D1	1.5	Const.	7.641 [0.9635]	79.81	93.04	77.28
D2	1.5	Const.	12.333 [0.9548]	76.76	165.98	99.68
D3	1.5	Const.	11.891 [0.9515]	76.99	162.00	97.81
C1	3.0	Const.	12.974 [0.9719]	80.69	163.02	98.61
C2	3.0	Const.	12.147 [0.9681]	77.71	153.67	93.19
C3	3.0	Const.	12.429 [0.9513]	77.69	152.81	93.00
L1	0	Const.	11.186 [0.9740]	69.81	162.29	98.17
L2	0	Const.	11.154 [0.9609]	75.14	151.70	91.35
L3	0	Const.	11.429 [0.9793]	69.50	164.78	98.75

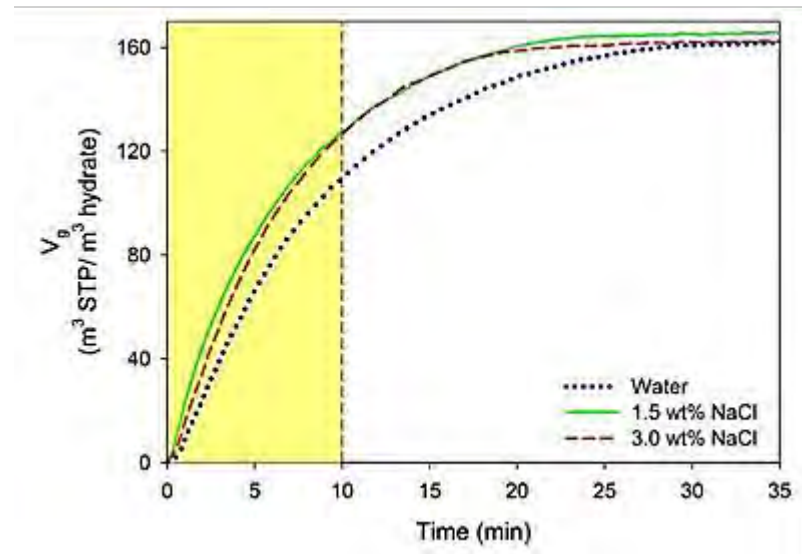


**Figure 2.10** Methane release curve from hydrates formed in water, 1.5 wt% NaCl and 3.0 wt% NaCl (Chong *et al.*, 2015).

Furthermore, they proposed the comparative of 1.5 wt%, 3.0 wt% NaCl, and water system as hydrate dissociation which shows in Figure 2.10. They found that the dissociation rates in salt solution were higher than water solution system because the presence of NaCl improved the dissociation rate because the salt ions especially  $\text{Cl}^-$  were embedded into water cage and attracted the H atoms from water molecules. Thereby, the original hydrogen bonding that formed the cages were disturbed in salt solution system. For the water system, methane dissolved more uniformly in the liquid phase. So, there was a higher methane concentration gradient between hydrate phase and surrounding liquid phase which drove a faster dissociation rate but it was still lower than the salt solution systems.

Sun *et al.* (2003) investigated the effect of additives on gas storage in methane hydrate which are anionic surfactant (Sodium Dodecyl Sulfate (SDS)), nonionic surfactant (Alkyl Polysaccharide Glycoside (APG)), and liquid hydrocarbon (Cyclopentane (CP)). The comparing effects of adding SDS and APG were shown in Figure 2.11.

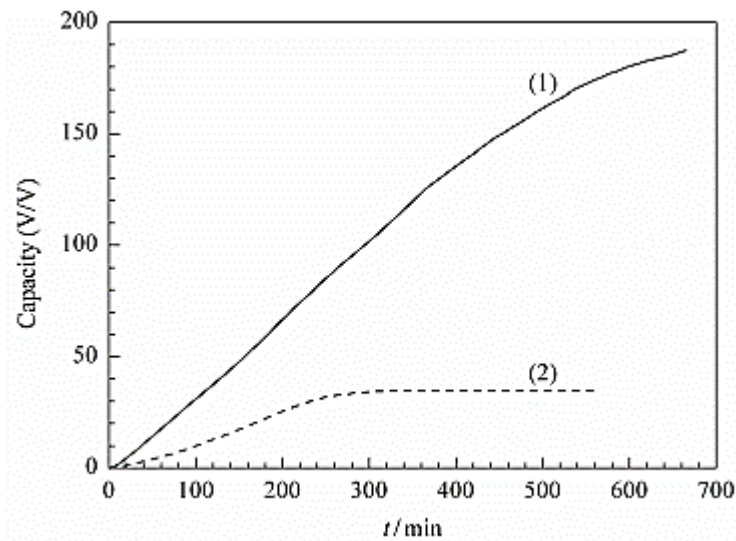


**Figure 2.11** Effects of different surfactants on methane hydrate formation (1)  $300 \times 10^{-6}$  SDS, (2)  $500 \times 10^{-6}$  APG; Reaction conditions:  $p = 4.34$  MPa,  $T = 274.05$  K (Sun *et al.*, 2003).

The hydrate formation rate in APG system was almost equal to SDS system during the formation step but the time of hydrate growth of APG system was shorter than SDS system. Thus, the adding of SDS on methane storage by hydrates formation was more practical when compared to APG. The comparison effects of surfactant were illustrated in Table 2.4.

**Table 2.4** Experimental results of methane storage in hydrates (Sun *et al.*, 2003)

No	Additive	$T/K$	$p/MPa$	Experimental time cost (min)	Storage capacity (V/V)	
1	SDS	274.05	5.54	330	163	
2			4.85	425	154	
3			4.34	460	147	
4			3.92	765	132	
5	APG	277.55	5.76	665	153	
6			5.33	705	146	
7			4.85	760	113	
8			5.38	455	112	
9			4.96	370	101	
10			4.34	285	80	
11	SDS+CP	274.05	6.18	315	169	
12			4.85	340	151	
13			3.80	540	129	
14			277.55	5.80	480	152
15				5.43	595	149
16				4.85	590	115

Solution concentration: DPG= $500 \times 10^{-6}$ , SDS= $300 \times 10^{-6}$ , CP=1.0%



For the results, adding SDS and APG into system not only decreased the hydrate induction time but also improved the hydrate formation rate and gas storage capacity. Furthermore, CP had similarly effect SDS and APG but it is not support methane storage in hydrates.

Prasad *et al.* (2014) explained the enhancement in methane storage capacity of gas hydrates formed in hollow silica. From Figure 2.12, it was clearly seen that the systems with silica had higher hydrate yield than the system without silica. Furthermore, it also rapidly increased at pressure around 4-5 MPa. Thus, rapid methane gas storage in the form of hydrates was possible at moderate pressures by using a hollow silica matrix. Moreover, hollow silica had a lot of advantages such as no special sample preparation and reusability for several hydrate formation and dissociation cycles.

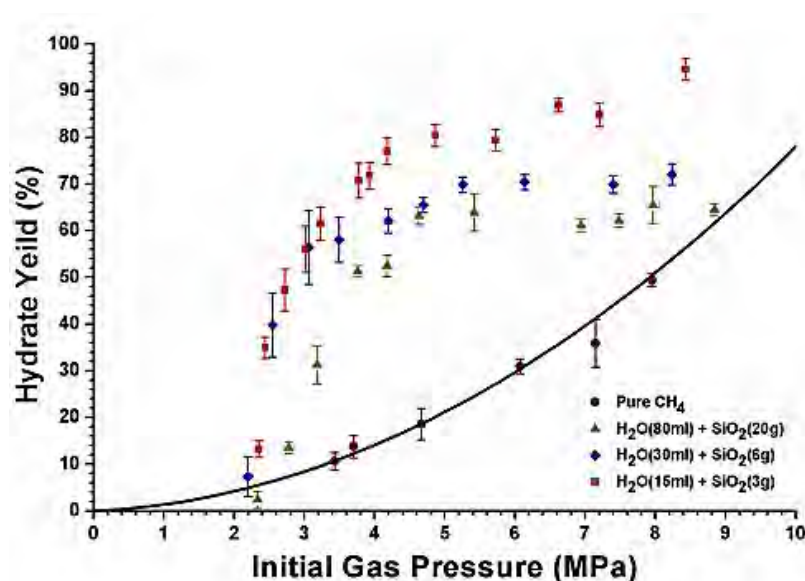


**Figure 2.12** Gas hydrate yield at different initial pressure in methane-water-silica systems (Prasad *et al.*, 2014).

Mekala *et al.* (2014) studied the formation and dissociation kinetics on methane hydrates which included Toyoura silica sand (particles size around 100-500  $\mu\text{m}$ ) with pure water at 8 MPa and seawater at 8 and 10 MPa and 277.15 K. Table 2.5 shows the water conversion to hydrate of pure water system and seawater system

which were 71.9 % and 11.6 % respectively. Figure 2.13 shows the gas uptake curves of pure water and seawater results at the same pressure and temperature. They concluded that the gas uptake results in pure water system were significantly higher than the seawater system.

**Table 2.5** Hydrate Formation Experiments Conducted at 277.2 K (Mekala *et al.*, 2014)

experiment number <sup>a</sup>	solution state <sup>b</sup>	pressure (MPa)	solution saturation (%) in porous media	induction time (min)	gas consumed at the induction point (mol of gas/mol of water)	gas consumption at the end of the experiment		water conversion (%)
						time (h)	gas uptake (mol of gas/mol of water)	
D1	F	8	100	0.3	0.00025	93.47	0.1182	72.07
D2	M	8	100	258.3	0.00154	91.97	0.1191	72.63
D3	M	8	100	25.7	0.00036	100.64	0.1179	71.90
D4	M	8	100	0.3	0.00011	68.43	0.1161	70.81
S1	F	8	100	3.7	0.00128	28.98	0.0119	7.25
S2	M	8	100	8.0	0.00110	89.32	0.0190	11.59
S3	M	8	100	9.0	0.00019	21.72	0.0100	6.09
S4	F	8	100	15.7	0.00135	23.61	0.0092	5.61
S5	M	8	100	21.0	0.00093	30.57	0.0073	4.45
S6	F	8	100	36.3	0.00368	26.26	0.0127	7.72
S7	F	10	100	2.0	0.00248	36.72	0.0191	11.63
S8	F	10	100	9.3	0.00037	15.73	0.0086	5.25
S9	F	10	75	8.0	0.00009	67.04	0.0519	31.66
S10	F	10	75	21.7	0.00359	67.44	0.0414	25.23
S11	M	10	75	0.3	0.00165	22.09	0.0361	22.04

<sup>a</sup>D, pure water; S, seawater. <sup>b</sup>F, fresh; M, memory.

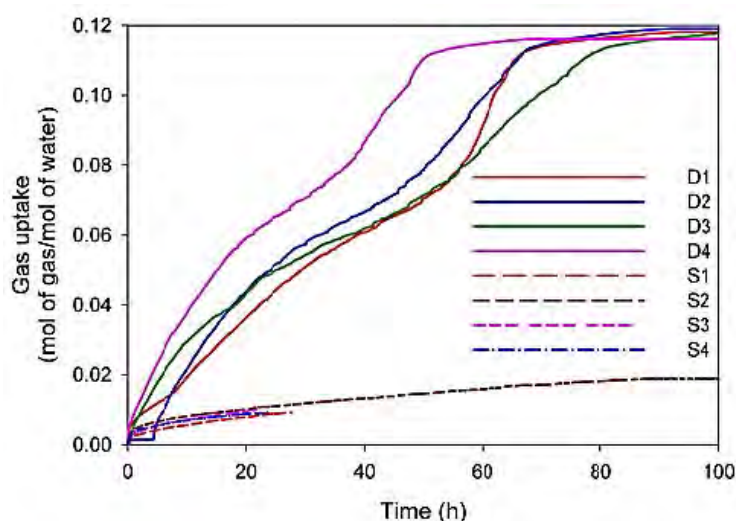


**Figure 2.13** Comparison of gas uptakes of pure water and seawater experiments at 8 MPa and 277.2 K (Mekala *et al.*, 2014).

The formation rates of hydrates were shown in Figure 2.14. They found that the average hydrate formation rate in pure water system was higher than seawater system, which was closed to zero in a few hours, because the presence of salt are not only alter the thermodynamics but also the kinetics growth which reacts as inhibitor. In addition, the seawater system reduced 10 times of gas uptake and rate of hydrates formation.

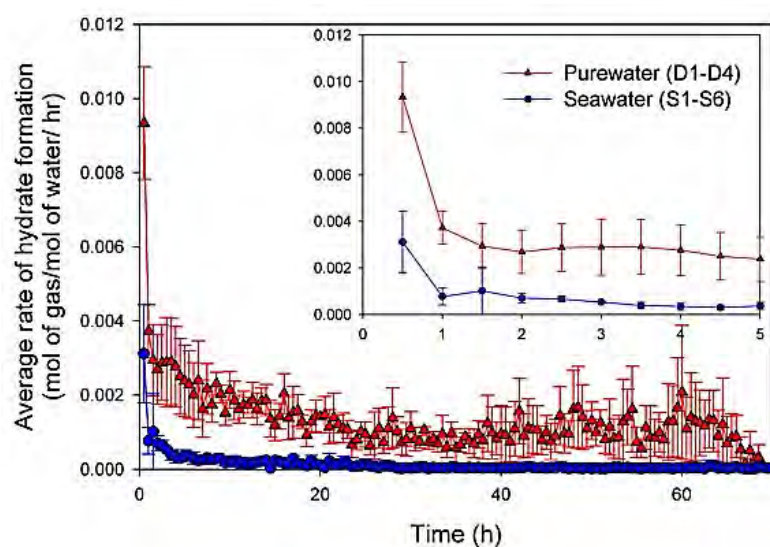


**Figure 2.14** Comparison of the average rate of hydrate formation between seawater and pure water experiments (Mekala *et al.*, 2014).

Figure 2.15 shows the gas release profile of pure water system and seawater system. They found that the hydrate dissociation rate of pure water system and seawater system took around 60 and 40 minutes respectively to complete the hydrates dissociation due to the extensive hydrate formation in pure water take a longer time to complete dissociation.

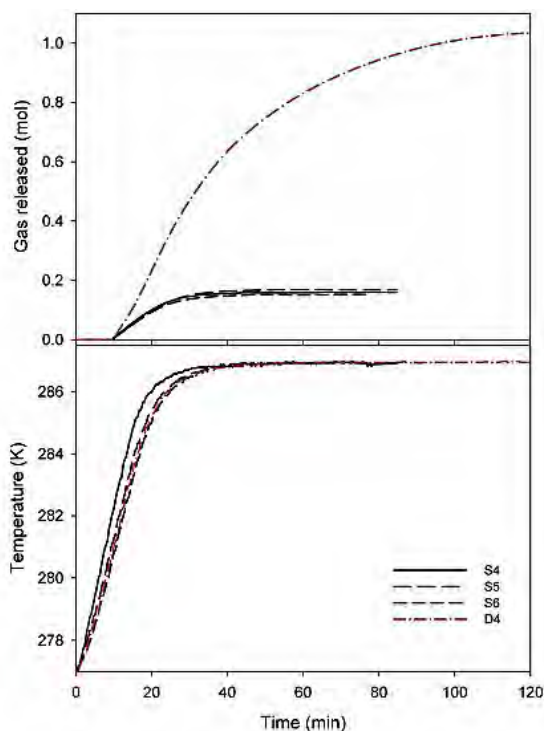


**Figure 2.15** Comparison of the number of gas moles recovered from hydrates of seawater and pure water at 4.8 MPa (Mekala *et al.*, 2014).

Chari *et al.* (2015) observed the methane hydrate formation in two different types of silica compared with pure methane. They investigated effects of stirring and non-stirring reactor. Pure silica, solid silica, and hollow silica were used as a porous media in stirred reactors. The methane hydrate formation was found to be the minimum in solid silica and maximum in hollow silica. For non-stirred reactor systems, the hydrate formation in pure silica and solid silica were almost neglect when compared to hollow silica as well as the kinetics and hydrate yield. Therefore, type of silica played an important role in hydrate formation. Furthermore, the fast hydrate formation, kinetics and high hydrate yield of hollow silica in non-stirring reactor decreased the energy and cost of synthesis the hydrate efficiently. Thus, the hollow silica could be considered as an advantage for storage and transportation of methane gas hydrate.

Zhang *et al.* (2016) observed the behaviors of methane hydrate in porous silica gels with different temperature from 267.15 to 278.15 K. Particle diameter and pore diameter were illustrated in Table 2.6. The particle diameter were applied for

porous silica experiments which diameter from 0.300 to 0.450 mm, 0.150 to 0.200 mm, and 0.105 to 0.150 mm. The effects of particle diameter were shown in Figure 2.16.

**Table 2.6** The experimental conditions and results (Zhang *et al.*, 2016)

Items	T/K	P <sub>g</sub> /MPa	n <sub>0</sub> /mol	Water conversion/mol%	Items	T <sub>g</sub> /K	P <sub>g</sub> /MPa	n <sub>0</sub> /mol	Water conversion/mol%
Pore diameter: 12.95 nm; Particle diameter range: 0.300–0.450 mm									
1	267.15	4.0	0.149	11.14	12	274.15	9.4	0.439	32.84
2	267.15	5.0	0.265	19.82	13	275.15	7.4	0.165	12.34
3	267.15	6.0	0.383	28.65	14	275.15	8.4	0.271	20.27
4	269.15	4.0	0.111	8.30	15	275.15	9.4	0.375	28.05
5	269.15	5.0	0.203	15.18	16	276.15	7.4	0.125	9.35
6	269.15	6.0	0.315	23.56	17	276.15	8.4	0.204	15.26
7	271.15	4.0	0.065	4.86	18	276.15	9.4	0.320	23.94
8	271.15	5.0	0.136	10.17	19	277.15	7.4	0.095	7.11
9	271.15	6.0	0.233	17.43	20	277.15	8.4	0.146	10.92
10	272.15	6.0	0.203	15.18	21	277.15	9.4	0.224	16.75
11	273.20	6.0	0.154	11.52	22	278.15	9.4	0.161	12.04
Pore diameter: 12.95 nm; Particle diameter range: 0.150–0.200 mm									
23	267.15	6.0	0.399	29.84	28	275.15	9.4	0.400	29.92
24	269.15	4.0	0.102	7.63	29	276.15	7.4	0.110	8.23
25	269.15	5.0	0.207	15.48	30	276.15	8.4	0.210	15.71
26	269.15	6.0	0.327	24.46	31	276.15	9.4	0.313	23.41
27	271.15	6.0	0.247	18.47	32	277.15	9.4	0.238	17.80
Pore diameter: 12.95 nm; Particle diameter range: 0.105–0.150 mm									
33	267.15	6.0	0.393	29.40	38	275.15	9.4	0.420	31.41
34	269.15	4.0	0.096	7.18	39	276.15	7.4	0.100	7.48
35	269.15	5.0	0.217	16.23	40	276.15	8.4	0.200	14.96
36	269.15	6.0	0.321	24.01	41	276.15	9.4	0.314	23.49
37	271.15	6.0	0.247	18.47	42	277.15	9.4	0.240	17.95
Pore diameter: 9.03 nm; Particle diameter range: 0.105–0.150 mm									
43	275.15	10.4	0.227	16.98	46	276.15	11.1	0.203	15.18
44	276.15	9.4	0.101	7.55	47	277.15	10.4	0.102	7.63
45	276.15	10.4	0.111	8.30					
Pore diameter: 17.96 nm; Particle diameter range: 0.105–0.150 mm									
48	267.15	6.1	0.424	31.71	54	275.15	9.4	0.490	36.65
49	269.15	3.1	0.066	4.94	55	276.15	7.4	0.245	18.33
50	269.15	4.1	0.166	12.42	56	276.15	8.4	0.333	24.91
51	269.15	5.1	0.270	20.20	57	276.15	9.4	0.427	31.94
52	269.15	6.1	0.375	28.05	58	277.15	9.4	0.361	27.00
53	271.15	6.1	0.324	24.23					
Pore diameter: 33.2 nm; Particle diameter range: 0.105–0.150 mm									
59	269.15	4.1	0.181	13.54	64	276.15	6.4	0.221	16.53
60	269.15	5.1	0.306	22.89	65	276.15	7.4	0.337	25.21
61	269.15	6.1	0.433	32.39	66	276.15	8.4	0.457	34.18
62	271.15	4.1	0.155	11.59	67	276.15	9.4	0.570	42.63
63	275.15	7.4	0.385	28.80	68	277.15	7.4	0.287	21.47

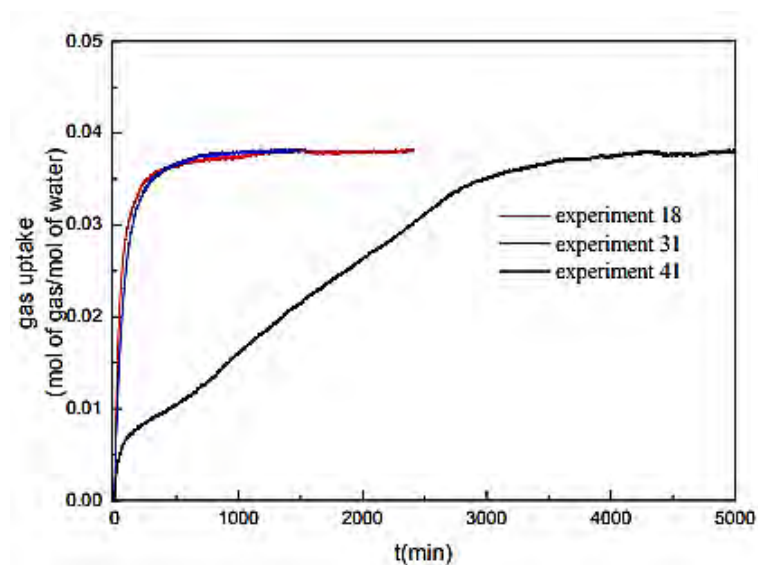


**Figure 2.16** Gas uptake curves of the hydrate formation in silica gels with the various particle diameter ranges at the bath temperature of 276.15 K and the initial pressure of 9.4 MPa (Zhang *et al.*, 2016).

From Figure 2.16, they found that the final gas uptake was not different for various particle diameters at the same temperature and initial pressure. So, the particle diameter had no an effect on final hydrate formation in silica gels. Figure 2.17 shows the effect of pore diameters of the silica gels. The gas uptake with various pore diameters at the same particle diameters range, initial pressure, and temperature was highest at 33.2 nm (experiment 67) because the equilibrium hydrate formation pressure decreases with the increase of the pore size. From Figure 2.17 and Table 2.6, they concluded that when the pore diameters were increased the rate of gas uptake would also increase. Because the driving force of the hydrate formation increased with increasing of the pore diameter resulting to the increasing of the gas uptake rate, the final gas consumption, and the decreasing of the final pressure.

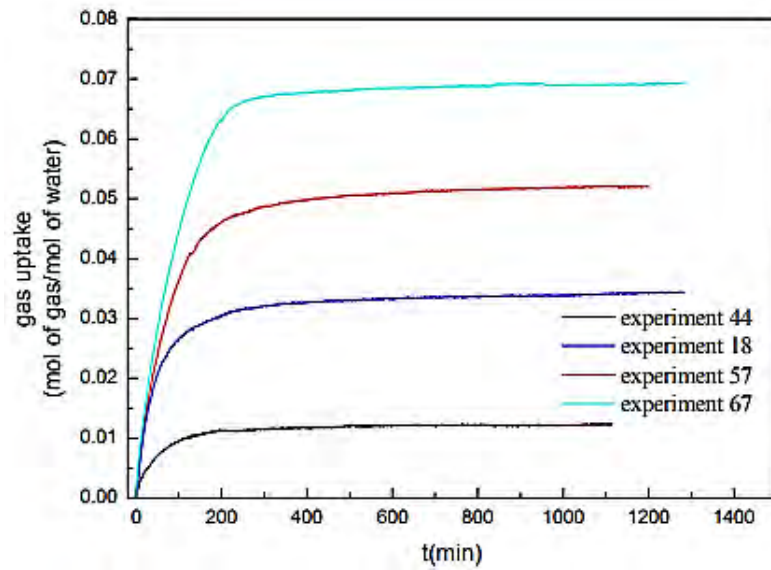


**Figure 2.17** Gas uptake curves of the hydrate formation in silica gels with various pore diameters and the particle diameter range of 0.105-0.150 mm at the temperature of 276.15 K and the initial pressure of 9.4 MPa (Zhang *et al.*, 2016).

Moreover, the methane uptake rate was increased with the decreasing of the temperature and increasing of the initial pressure and mean pore diameter but slightly affected by the particle diameter.

Siangsai *et al.* (2015) investigated the roles of activated carbon particle sizes on methane hydrate formation and dissociation. The activated carbon sizes were observed in difference particle sizes from 250 to 420  $\mu\text{m}$ , 420 to 841  $\mu\text{m}$  and 841 to 1680  $\mu\text{m}$  at 8 MPa and 277 K in a quiescent fixed bed crystallizer.

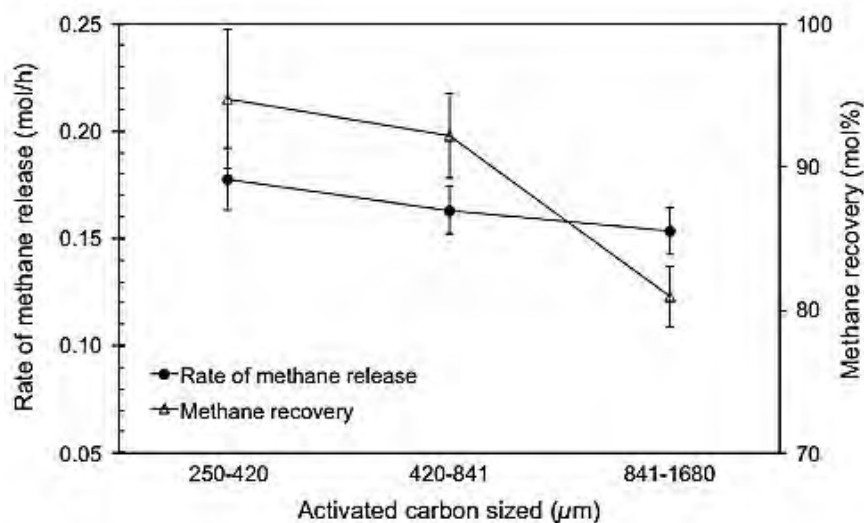


**Figure 2.18** Comparison of the rate of methane release and methane recovery from the hydrate dissociation experiment carried out at 8 MPa and  $\Delta T=294$  K (Siangsai *et al.*, 2015).

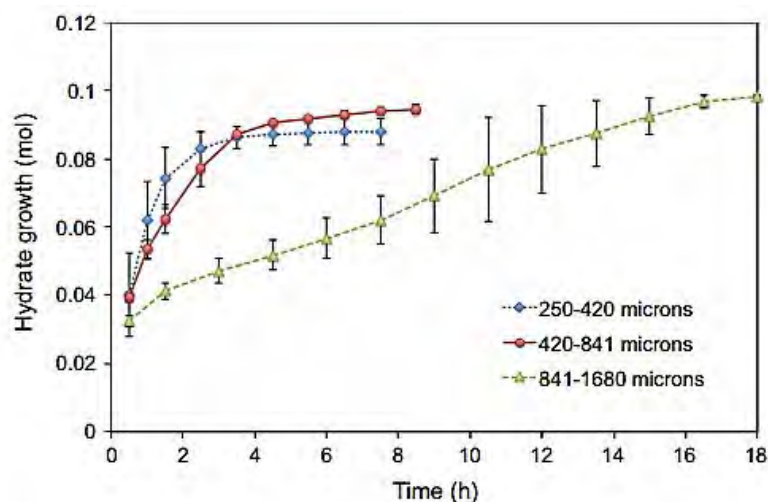


**Figure 2.19** Comparison of the average hydrate growth during the methane hydrate formation at 8 MPa and 277 K with the activated carbon particle sizes of 250– 420  $\mu\text{m}$ , 420– 841  $\mu\text{m}$ , and 841–1680  $\mu\text{m}$  (Siangsai *et al.*, 2015).

Figures 2.18 and 2.19 show the effects of activated carbon sizes on the methane hydrate formation and dissociation. They conclude that the activated carbon



sizes from 250 to 420  $\mu\text{m}$  was the fastest methane hydrate consumption due to the smaller activated carbon sizes would increase the contact area between methane gas and water through the interconnected space between the activated carbon particles. Moreover, this activated carbon size exhibited the highest methane recovery in the methane hydrate dissociation experiment. Nonetheless, the activated carbon size from 841 to 1680  $\mu\text{m}$  showed the highest methane consumption and water conversion to hydrate because of a large interstitial space between the activated carbon particles.

Celzard and Mareche, (2005) observed the methane hydrate storage within wet commercial activated carbons which have wetting ratio (R) around 1 ( R = mass ratio water/carbon). This experiment was investigated at 275 K and up to 8 MPa. They also studied the pore volume of activated carbon by water saturation at below the formation pressure and low temperature (close to 273 K) condition. It was clearly seen that the hydrate formation at the lowest possible pressure was not act as a good gas storage and slowed down the formation kinetics due to the presence of water which blocking of the throughout porosity. Although the porous media were uniformly spreaded in water, the methane hydrates formation was quite low. The presence of an additive or promoter such as sodium dodecyl sulphate (SDS) would enhance the hydrate formation rate at low pressure but the final gas storage was not higher than the system without SDS.

Veluswamy *et al.* (2016) studied the effect of promoter such as tetrahydrofuran (THF) to rapidly promote methane hydrates formation and develop the cost effective in large scale of energy storage system. They varied experimental conditions and THF concentration to get the suitable condition for enhance rapidly methane hydrates formation by using unstirred tank reactor (UTR). Figure 2.20 shows the curves of methane gas uptake of THF system and pure water system with different pressure and temperature.

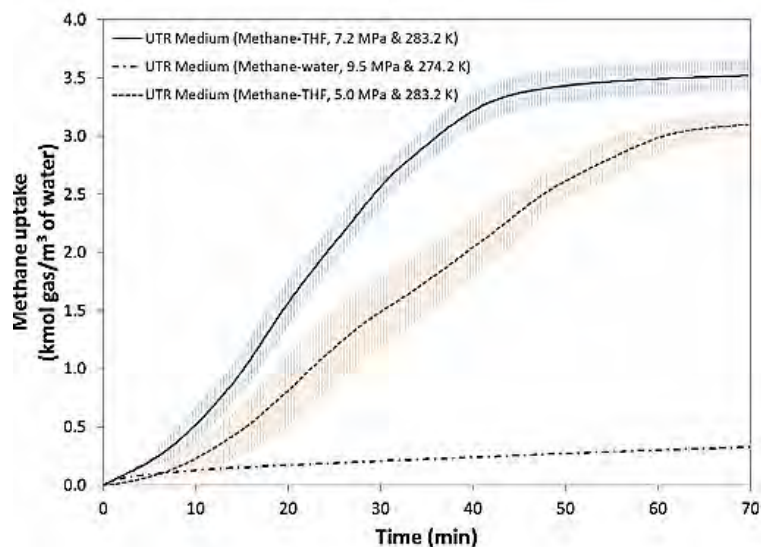


**Figure 2.20** Enhanced methane uptake by adding THF as a promoter in a UTR (Veluswamy *et al.*, 2016)

They proposed that the UTR system with the presence of THF as a promoter had a higher methane gas uptake than pure water system. In 1 hour, the methane uptake of THF system was enhanced 11 times higher than the pure water system. Even though a low pressure of THF system at 5 MPa and 283.2 K, THF system still achieved a capacity 9 times of pure water system. Moreover, they compared the particular presence of THF system which different initial pressure. The result showed that the system with THF and higher initial pressure was the highest methane uptake and performed the rapid kinetics due to the distinct hollow crater supported by well-connected channels for fluid flow and driving force. Therefore, the presence of promoter like tetrahydrofuran (THF) mixed with water in the process of hydrate formation could enhance both thermodynamics and kinetics performance which able to develop a low cost and energy efficient of solid natural gas technology via clathrate hydrates for natural gas storage.

Linga *et al.* (2009) reported the three different sizes and volume beds of silica sand particles in gas hydrates formation to study the behavior of gas in the interstitial space of silica sand bed particles. The average sand particles was 329  $\mu\text{m}$  and the experiments were conducted at 6.2 MPa and varied temperature of 280, 277, and 274 K. They found that water conversion to hydrate at 277 and 274 K were more than 74% and showed the multiple nucleation point by verifying of hydrate formation in the sand was achieved via Raman spectroscopy and morphology. Furthermore, they studied the effect of silica sand bed sizes by installing one and two copper cylinders in the crystallizer reactor. Figure 2.21 shows the results which adding copper cylinders.

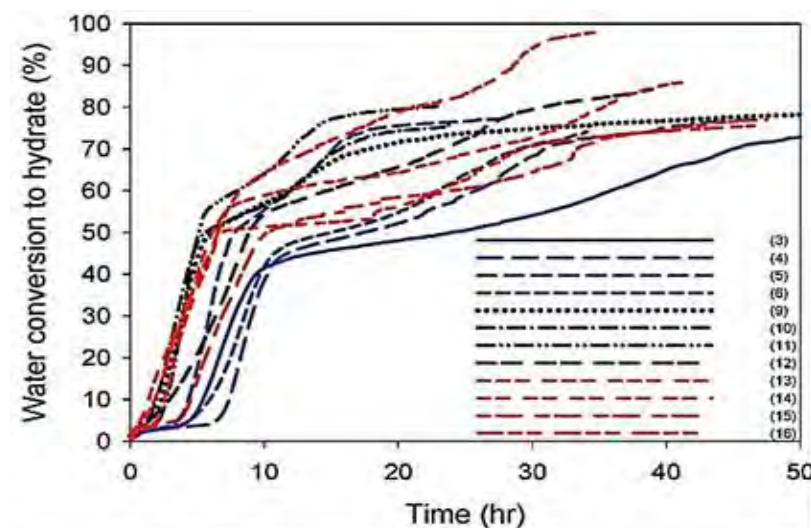


**Figure 2.21** Percentage of water to hydrate conversion for all of the formation experiments conducted at 277 K and three different bed sizes. Time zero represents the nucleation point. Blue color lines represent the experiments for the largest bed size (CR). Black color lines represent the experiments for the medium bed size (CR + CC1). Red color lines represent the experiments for the smallest bed size (CR + CC1 + CC2) (Linga *et al.*, 2009).

The result shows the initial slow growth rate of 43 to 53 % of converted water to hydrate. After that, the third and final growth stage were increased in the range of 74 to 98% conversion and gas uptake dynamics changed. It can be concluded that the hydrate formation rate in porous bed depend on the size of the bed.

Chari *et al.* (2013b) observed the methane hydrates formation and dissociation in pure water system and nano silica suspension system in non-stirred reactor. The methane hydrate yield in the presence of nano silica system improved the methane hydrate conversion more than 80%. The system with nano silica powder (weight ratio SiO<sub>2</sub> to H<sub>2</sub>O is 1:4) could promote and increase in the gas-water interfacial surface area by forming a dispersed water phase at ambient temperature. Therefore, this enhancement could increase the methane hydrate formation kinetics and hydrate conversion which indicated the optimal silica to water ratio and essential for hydrate conversion.

## **CHAPTER III**

### **EXPERIMENTAL**

#### **3.1 Materials and Equipment**

##### 3.1.1 Materials

1. Hollow silica (99 % P-type purchased from Nanoshell, India)
2. Activated carbon (supported by Carbokarn Co., LTD., Thailand)
3. Ultra high purity methane gas (99.999% purity from Labgaz Co., Ltd., Thailand)
4. Deionized water

##### 3.1.2 Equipments

- a. Hydrate formation/dissociation apparatus
  1. Crystallizer (CR)
  2. Reservoir (R)
  3. Personal Computer (PC)
  4. Pressure transducer (PT)
  5. K-type thermocouple
  6. Controllable water bath
- b. Surface area analyzer (Autosorb-1MP, Quantachrome)
- c. Surface area analyzer (Autosorb-1, Quantachrome)

#### **3.2 Experimental Procedures**

##### 3.2.1 Experimental Apparatus

Figure 3.1 shows the schematic and cross section of gas hydrate apparatus; the system consisted of a high pressure stainless steel crystallizer (CR), a reservoir (R), and a crystallizer. The reservoir was immersed in a cooling bath, the temperature of which was adjusted and controlled by an external controllable circulator. The pressure transducers were used to measure the pressure. The temperature in the crystallizer was measured by using k-type thermocouples (Siangsai

*et al.*, 2015). Figure 3.1b shows the cross section of crystallizer, where the thermocouples were located: T1 at the top of the bed, T2 at the middle of the bed, T3 at the bottom of the bed, and T4 at the bottom of the crystallizer. The pressure and temperature profiles were obtained by using a data logger (AI210 Model, Wisco Industrial instruments, Thailand).

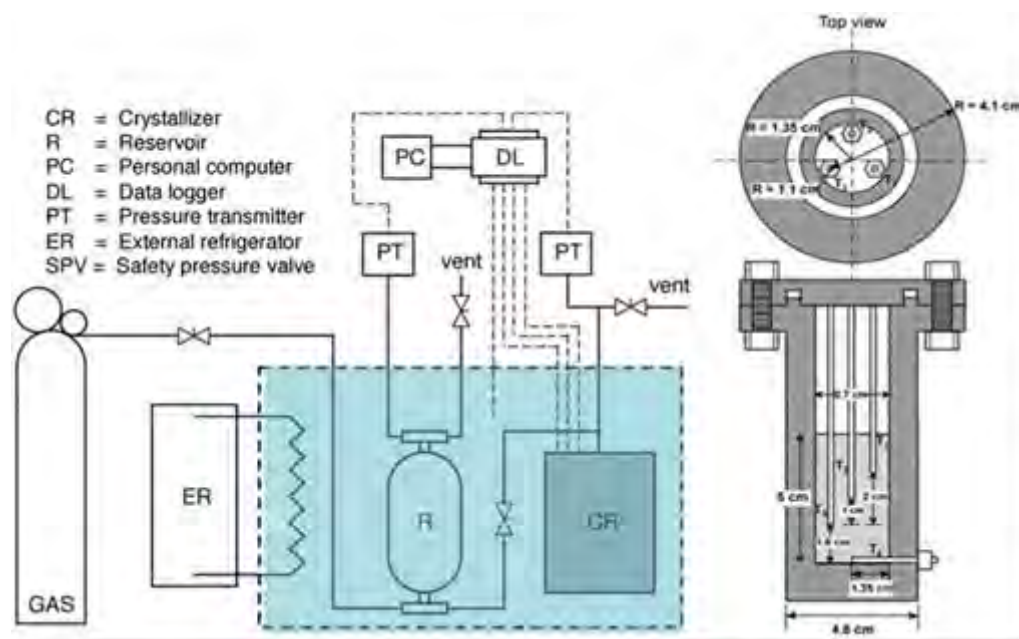


**Figure 3.1** Schematic diagram of gas hydrate apparatus; a) schematic diagram, b) cross-section of a crystallizer (Siangsai *et al.*, 2015).

### 3.2.2 Methane Hydrate Formation

The experimental apparatus was cleaned using deionized water and purged with methane to ensure that the reactor was thoroughly clean, and evacuated with a vacuum pump before each experiment. After that, the reactor was cooled until temperature was stabilized. Methane gas was introduced into the system rapidly after the temperature steady from SV until the system pressure reached the desired experimental pressure (8 MPa). The data was then recorded every 10 seconds. All experiments were carried out in the quiescent condition with a fixed amount of water and gas in the system. During the hydrate formation, the pressure in the CR was reduced due to the gas consumption, and the temperature was increased due to the

effect of exothermic reaction. The experiments continued until no significantly change in the pressure. The pressure and temperature data was used to calculate for the methane consumption (gas uptake) using the following Equation 3.1 (Babu *et al.*, 2014).

$$\Delta n_{H,\downarrow} = n_{H,t} - n_{H,0} = \left(\frac{PV}{zRT}\right)_{G,0} - \left(\frac{PV}{zRT}\right)_{G,t} \quad (3.1)$$

where  $\Delta n_{H,\downarrow}$  = moles of consumed gas for hydrate formation (mole)

$\Delta n_{H,t}$  = moles of hydrate at time t, (mole)

$\Delta n_{H,0}$  = moles of hydrate at time 0, (mole)

P = pressure of the crystallizer, (atm)

T = temperature of the crystallizer, (K)

V = the volume of gas phase in the crystallizer, (cm<sup>3</sup>)

Z = compressibility factor

R = the universal gas constant 82.06 cm<sup>3</sup> atm/mol K

Subscripts of G, 0 and G, t represent the gas phase at time zero and time t respectively. The conversion of water to hydrate is calculated by Equation (3.2) (Babu *et al.*, 2014).

$$\text{Conversion of water to hydrates} = \frac{\Delta n_{H,\downarrow} \times \text{hydration number}}{\Delta n_{H_2O}} \times 100 \quad (3.2)$$

where  $\Delta n_{H_2O}$  = moles of water in the system, mol

$\Delta n_{H,\downarrow}$  = moles of consumed gas for hydrate formation, mol

Hydration number is the number of water molecules per gas molecules.

### 3.2.3 Methane Hydrate Dissociation

After methane hydrate formation, the hydrates were dissociated by using thermal stimulation (increase temperatures). The pressure in the crystallizer was decreased to the desired pressure by venting out the free gas in the system. Then, the temperature was increased from the formation temperature to desired dissociation

temperature. This point was marked as time zero for the hydrate dissociation experiments. The total moles of gas in the system equaled to the moles of gas at time zero. At any given time, the total number of moles ( $n_{T,t}$ ) in the system remained constant and equaled to that at time zero ( $n_{T,0}$ ). Therefore, the mole of released methane from the hydrate at any time during the hydrate dissociation was calculated by Equation (3.3) (Siangsai *et al.*, 2015).

$$\Delta n_{H,\uparrow} = n_{H,0} - n_{H,t} = \left( \frac{PV}{zRT} \right)_{G,t} - \left( \frac{PV}{zRT} \right)_{G,0} \quad (3.3)$$

where  $\Delta n_{H,\downarrow}$  = moles of consumed gas for hydrate formation (mole)

$\Delta n_{H,t}$  = moles of hydrate at time  $t$ , (mole)

$\Delta n_{H,0}$  = moles of hydrate at time 0, (mole)

$P$  = pressure of the crystallizer, (atm)

$T$  = temperature of the crystallizer, (K)

$V$  = the volume of gas phase in the crystallizer, ( $\text{cm}^3$ )

$Z$  = compressibility factor

$R$  = the universal gas constant  $82.06 \text{ cm}^3 \text{ atm/mol K}$

Subscripts of G, 0 and G,  $t$  represent the gas phase at time zero and time  $t$  respectively. The methane recovery was calculated by Equation (3.4) as a function of time for any dissociation experiment based on its information of formation experiment (Siangsai *et al.*, 2015).

$$\% \text{Methane recovery} = \frac{\Delta n_{H,\uparrow}}{\Delta n_{H,\downarrow}} \times 100 \quad (3.4)$$

where  $\Delta n_{H,\uparrow}$  = moles of consumed gas for hydrate dissociation, (mole)

$\Delta n_{H,\downarrow}$  = moles of consumed gas for hydrate formation, (mole)



## **CHAPTER IV**

### **RESULTS AND DISCUSSION**

In this work, hollow silica and activated carbon were selected as the porous media to investigate their effects and effects of the porous material to water ratio on the hydrate formation and dissociation. The experiments were conducted at 8 MPa and at 277 K in the quiescent condition. The dissociation experiments were observed after the completion of gas hydrate formation experiments. The thermal stimulation method was used in this research to dissociate gas hydrate by increasing temperature to 298 K.

#### **4.1 Effects of Hollow Silica**

##### 4.1.1 Methane Hydrate Formation

Table 4.1 presents the methane hydrate formation with the hollow silica (HSC) and water at 8 MPa and 277 K. The HSC was fixed at 1.5 g and water was varied to obtain 1:10, 1:12, and 1:14 HSC to water ratios. The system with the 1:12 HSC to water ratio is used as the system saturated with water, which the system with the 1:10 HSC to water ratio has about 20% less water from the 1:12 HSC to water ratio case. On the contrary, the 1:14 HSC to water ratio has 20% more water than the saturated case. The induction time used in this context means the interval between the establishment of super saturation and the formation critical nuclei as defined by Khurana *et al.* (2017). According to the table, the induction times of hydrate formation with the three different HSC water ratios are different. As the amount of water increases, the induction time increases. That is due to the reduction in the free headspace available for methane gas in the crystallizer (Prasad, 2015). Moreover, the increase in water increases both water conversion to hydrates and methane consumed. That is due to the increased amount of water available at interconnectivity and interstitial pore spaces between the HSC, which, in turn, increases the contact area between the gas and liquid phases. The high contact area between the two phases leading to the high quantity of gas dissolved into water.

Therefore, the amount of water does affect the hydrate formation kinetics, water conversion to hydrates, and methane consumed.

The formation of gas hydrates is an exothermic process, so it can be noticed by temperature spikes of thermocouples in the crystallizer. Figure 4.1 shows the gas uptake and temperature profiles during the methane hydrate formation of the HSC/H<sub>2</sub>O/CH<sub>4</sub> system at 1:10 HSC to water ratio (Experiment 3, Table 4.1). After the methane gas is introduced to the system, the gas uptake continuously increases due to the dissolution of methane gas into water. Then, the system remains in the gas hydrate stability zone until the hydrate nucleation occurs. The rate of gas uptake rapidly increases because the methane gas is consumed to form the hydrates until it reaches to the limit of hydrates formation.

Four thermocouples are located at different positions inside the crystallizer: T1 located at the top of the bed, T2 at the middle of the bed, T3 at the bottom of the bed, and T4 at the bottom of crystallizer. The temperature of the thermocouples in the crystallizer rises at T1 first. So, the methane hydrate formation with the presence of the HSC takes place at the top of the bed and grows to the other locations.

The gas uptake and temperature profiles during the methane hydrate formation of the HSC/H<sub>2</sub>O/CH<sub>4</sub> system at 1:12 HSC to water ratio (Experiment 5, Table 4.1) is shown in Figure 4.2. It can be seen that the methane gas up take is almost the same as the case with the 1:10 HSC to water ratio system. The methane hydrate growth in these two systems shows two step nucleations. First, the gas uptake increases rapidly as the result of the hydrate nucleation and its growth at the interface between gas and liquid phase. Second, the gas uptake increases again, which is noticed by the slope of the gas uptake and temperature rises, because the hydrate crystals may be cracked and water molecules could form methane hydrate again (Chari *et al.*, 2013a). Because a very low bulk density of HSC, it disperses on water, which could provide multiple nucleations and the gas easy to access the water available for hydrates (Veluswamy *et al.*, 2015).

**Table 4.1** Methane hydrate formation experimental conditions in the system with the presence of hollow silica at 8 MPa and 277 K

EXP. No.	#HSC to Water Ratio	Amount of Water Used [ml]	Experimental Pressure [MPa]	Experimental Temperature [°C]	*Induction Time [min]	CH <sub>4</sub> Consumed [mol/mol of H <sub>2</sub> O]	Water Conversion to Hydrates [%mol]
1	1:10	15	8	4	77.50	0.1323	80.56
2	1:10	15	8	4	47.00	0.1276	77.71
3	1:10	15	8	4	68.50	0.1329	80.92
					Average	0.1309±0.0029	79.73±1.75
4	1:12	18	8	4	69.83	0.1327	84.53
5	1:12	18	8	4	80.67	0.1475	84.83
6	1:12	18	8	4	85.50	0.1462	84.06
					Average	0.1421±0.0081	84.47±0.38
7	1:14	21	8	4	89.50	0.1687	88.19
8	1:14	21	8	4	200.11	0.1708	88.41
9	1:14	21	8	4	146.00	0.1706	88.30
					Average	0.1700±0.0012	88.30±0.11

#By weight

\*Induction Time = Time when the first hydrate was observed.

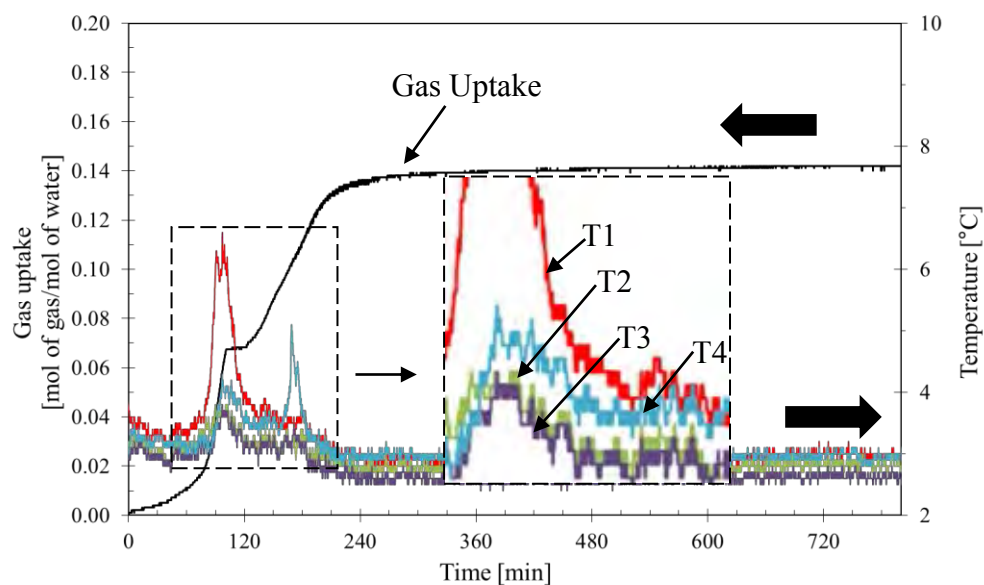


**Figure 4.1** Gas uptake and temperature profiles during the methane hydrate formation of the HSC/H<sub>2</sub>O/CH<sub>4</sub> system at 8 MPa and 277 K and 1:10 HSC to water ratio (Experiment 3, Table 4.1).

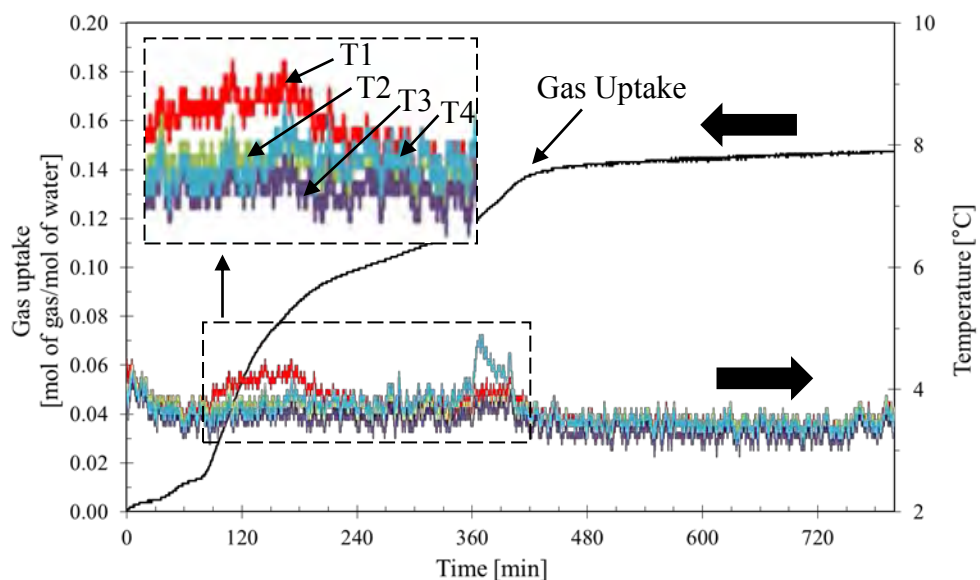


**Figure 4.2** Gas uptake and temperature profiles during the methane hydrate formation of the HSC/H<sub>2</sub>O/CH<sub>4</sub> system at 8 MPa and 277 K and 1:12 HSC to water ratio (Experiment 5, Table 4.1).

The gas uptake and temperature profiles during the methane hydrate formation of the HSC/H<sub>2</sub>O/CH<sub>4</sub> system at 1:14 HSC to water ratio is shown in Figure 4.3. It can be clearly seen that the methane hydrates take place in three steps. The first and second steps are similar to the 1:10 and 1:12 HSC to water ratio cases but there is an additional step for the 1:14 HSC to water ratio case. Jin *et al.*, (2012) reported that the third growth steps may occur by cracking the hydrate film, and induce water molecules to form the hydrates again. The temperature spike of the last step is not noticed because the temperature in the system is proportional to the extent of methane hydrate and heat transfer effects. It can be indicated that the methane hydrate, formed in the third step, has lower extent than that in the second step so the heat released from the methane hydrate formation was lower and easier to transfer than the second step. Thus, the third step of the methane hydrate formation not shows significant spikes in temperature profiles (Babu *et al.*, 2013).

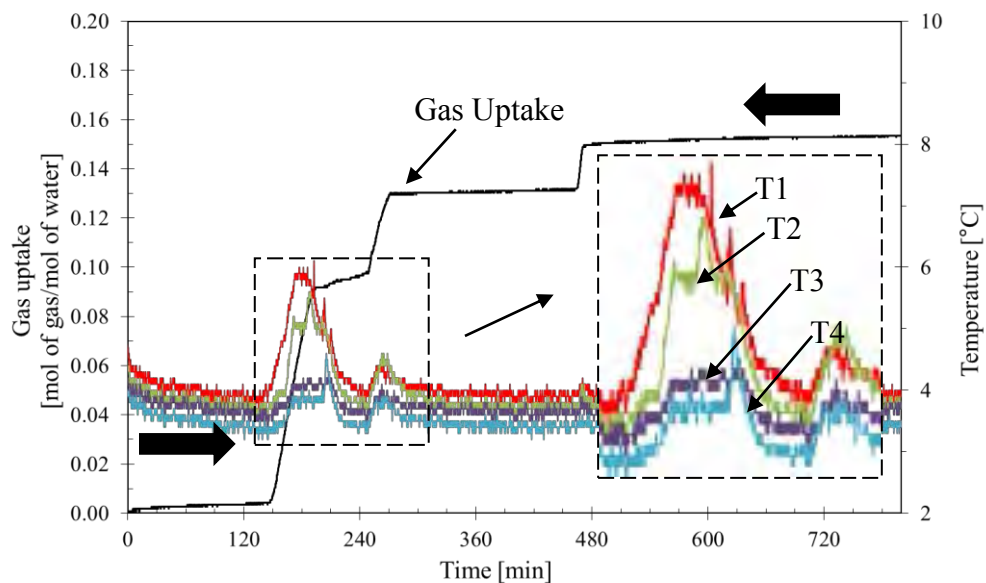


**Figure 4.3** Gas uptake and temperature profiles during the methane hydrate formation of the HSC/H<sub>2</sub>O/CH<sub>4</sub> system at 8 MPa and 277 K and 1:14 HSC to water ratio (Experiment 9, Table 4.1).

Scanning electron micrographs of the HSC are provided in Figure 4.4. The micrographs show the spherical hollow silica particles in the range of 30-70  $\mu\text{m}$  and smooth surface, which has a hollow core surrounded by a thin solid shell making HSC very light and low density, and high porosity (highly interconnected pore spaces) allowing it float above the water bed. Thus, the majority of hydrates form at the interconnectivity spaces could be the reason of the growth rate kinetics (Veluswamy *et al.*, 2015).

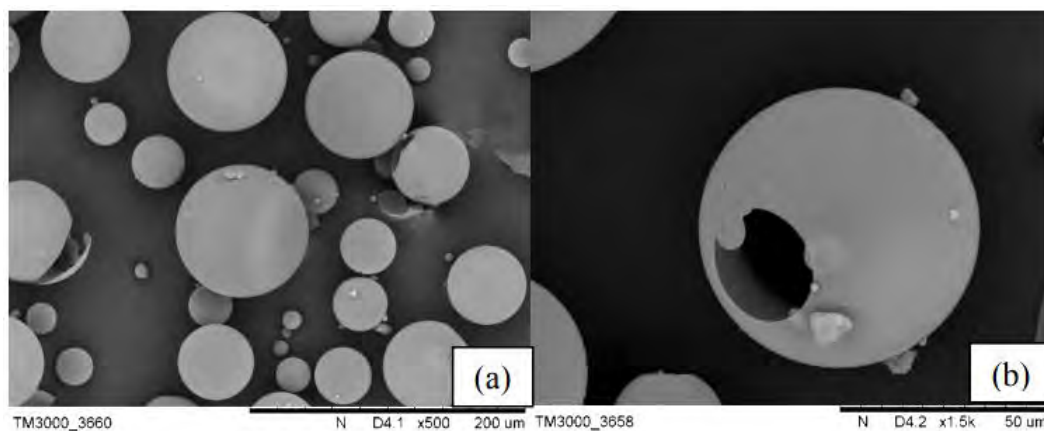


**Figure 4.4** Morphology of hollow silica by scanning electron microscope (SEM) (a) Particle of hollow silica in different sizes, (b) Breakage hollow silica (Suesuan, 2015).

Figure 4.5 presents the comparison of gas uptake rates during the methane hydrate formation in the system of HSC/H<sub>2</sub>O/CH<sub>4</sub> with different HSC to water ratios. After introducing the methane gas into the system, the gas dissolves into the water by passing through porous bed, which increases the contact area between gas and liquid phases. The 1:14 HSC to water ratio, which has excess water relative to the amount of HSC, shows the longest induction time due to the increase in the mass transfer resistance of water in the bed to the gas hydrate interfacial area for the hydrate growth and the decrease in the free headspace available for methane gas in the crystallizer. After that, the hydrate formation takes place. On the contrary, the other two ratios, 1:10 (deficit amount of water) and 1:12 (saturated amount of water) have about the same initial methane hydrate formation rate,  $0.0010 \pm 0.0004$  and  $0.0014 \pm 0.0007$  mol/ mol of H<sub>2</sub>O/ time, and the same induction time. For the system with the

1:10 HSC to water ratio, the hydrate formation rises rapidly after 60 minutes. That is because, in this case, the water level is below the HSC bed and that provides pathways for hydrates to grow better than in the 1:14 case, where the hydrates formed could block the methane hydrate formation from the gas and liquid interphase. The system with the 1:14 HSC to water ratio (excess amount of water) has the highest initial methane hydrate formation ( $0.0021 \pm 0.0003$  mol/ mol of  $H_2O$ / time) and water conversion to hydrates. The system with the 1:14 HSC to water ratio has the highest amount of water to fill both pores and interconnectivity spaces, which may contribute to multiple nucleation. In this case, the excess water located at the space between particles could result in the high water conversion to hydrates, hence, the high methane consumed. The methane consumed from the system with the 1:14 HSC to water ratio is 0.17 mol/ mol of  $H_2O$ , which is higher than that with the 1:10 and 1:12 HSC to water ratios, 0.13 and 0.14 mol/ mol  $H_2O$ , respectively. It can be concluded that the HSC to water ratio could affect the induction time, the hydrate formation rate, the water conversion to hydrates, and the methane consumed.

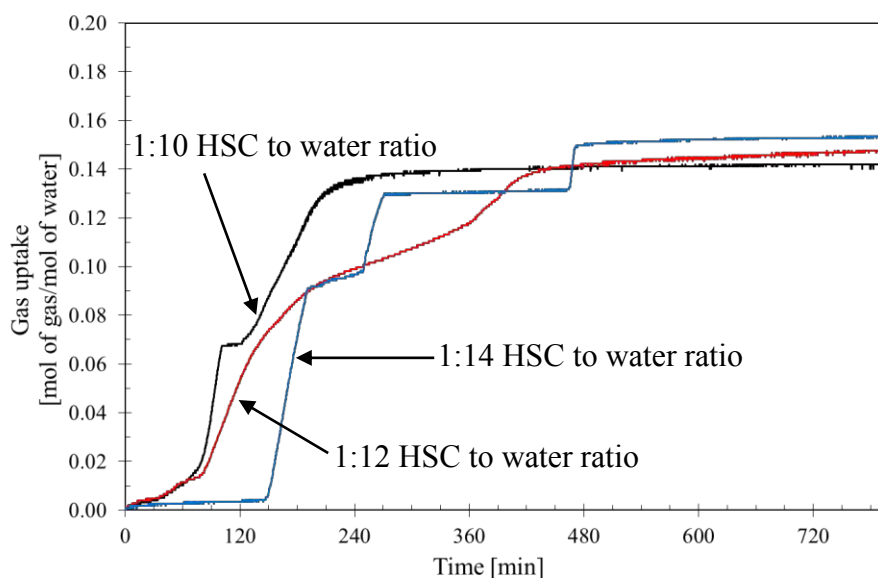


**Figure 4.5** Comparison of hydrate growth during the methane hydrate formation in the system of HSC/ $H_2O$ / $CH_4$  at 8 MPa and 277 K and various HSC to water ratios (1:10, 1:12, and 1:14). Time zero in the figure corresponds to the first point of hydrate growth.

#### 4.1.2 Methane Hydrate Dissociation

Decomposition of hydrates was performed by thermal stimulation with 294 K temperature driving force. Table 4.2 presents the methane hydrate dissociation of the system of HSC/H<sub>2</sub>O/CH<sub>4</sub> at different HSC to water ratios. The dissociation temperature ( $T_d$ ) is the first temperature that the methane gas releases from the hydrates. The methane released indicates the amount of methane emitted from the hydrate crystals, which is used to calculate the methane recovery. It can be noticed that the final methane recovery from the systems with the three different HSC to water ratios is not significantly different. Hence, the final methane gas is not affected by the HSC to water ratio. After methane hydrate dissociation, some methane gas still remains in the water, and it is not recovered, which was also reported by Linga *et al.* (2009).

Figures 4.6, 4.7, and 4.8 show the methane released and temperature profiles in the system of HSC/H<sub>2</sub>O/CH<sub>4</sub> with 1:10, 1:12, and 1:14 HSC to water ratios, respectively. After the methane hydrate formation process completes, the decomposition starts with thermal stimulation by increasing the temperature from 277 to 298 K (temperature driving force of 294 K). As shown in the figures, the majority of methane gas is released from 20 to 80 minutes. The thermocouple T1 takes the longest time for dissociation, which means that the methane hydrate formed is more stable at the top of the crystallizer than the other locations. Then, the methane recovery stops and all temperature profiles reach the plateau, 298 K. There is a small drop of temperature in the crystallizer, while methane gas is releasing. That may be due to the hydrate lump attached to the thermocouples T1 and T2, which can be noticed in the insets of Figures 4.6, 4.7, and 4.8. The decomposition from the systems with the three different water ratios have more or less the same methane released profile. Thus, at the same temperature driving force ( $\Delta T = 294$  K), the amount of water does not affect the methane released.



**Table 4.2** Methane hydrate dissociation experimental conditions in the system with the presence of hollow silica using  $^a\Delta T = 294$  K

EXP. No.	<sup>#</sup> HSC to Water Ratio	$\Delta T^a$ [°C]	Dissociation Temperature, $T_d^b$ [°C]	CH <sub>4</sub> Released [mol/mol of H <sub>2</sub> O]	CH <sub>4</sub> Recovery [%mol]
10	1:10	21	6.6	0.1272	96.11
11	1:10	21	7	0.1226	95.14
12	1:10	21	6.6	0.1280	96.32
			Average	0.1259±0.0029	95.86±0.62
13	1:12	21	6	0.1214	91.48
14	1:12	21	6.5	0.1319	89.37
15	1:12	21	6.2	0.1314	89.89
			Average	0.1282±0.0059	90.25±1.01
16	1:14	21	5.2	0.1592	94.34
17	1:14	21	5.2	0.1582	92.65
18	1:14	21	5.3	0.1583	92.81
			Average	0.1586±0.0006	93.27±0.93

<sup>#</sup>By weigh<sup>a</sup> $\Delta T = T_{\text{end}} - T_{\text{start}}$ <sup>b</sup> $T_d$  = Dissociation temperature

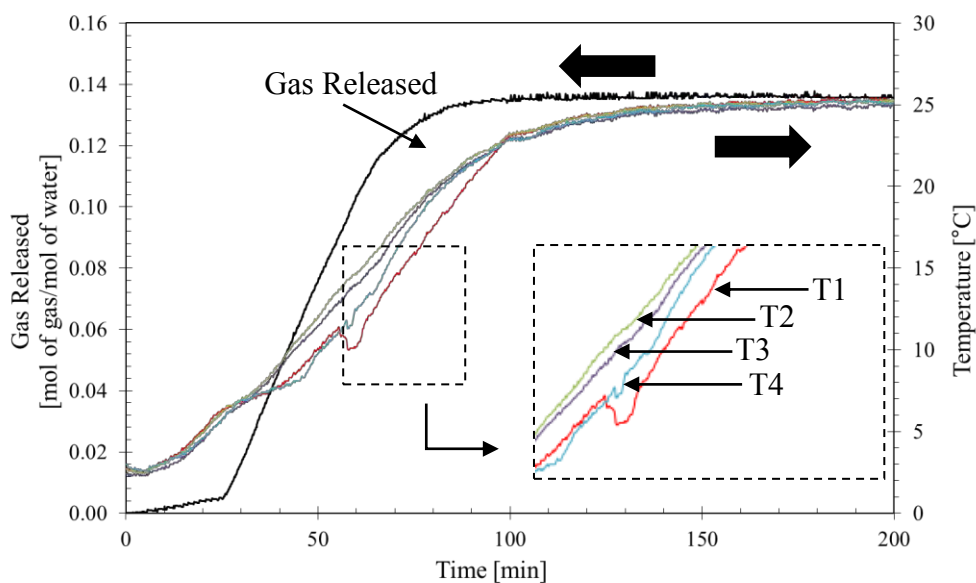


**Figure 4.6** Methane released and temperature profiles in the system of the HSC/H<sub>2</sub>O/CH<sub>4</sub> with the 1:10 HSC to water ratio and temperature driving force = 294 K (Experiment 12, Table 4.2).

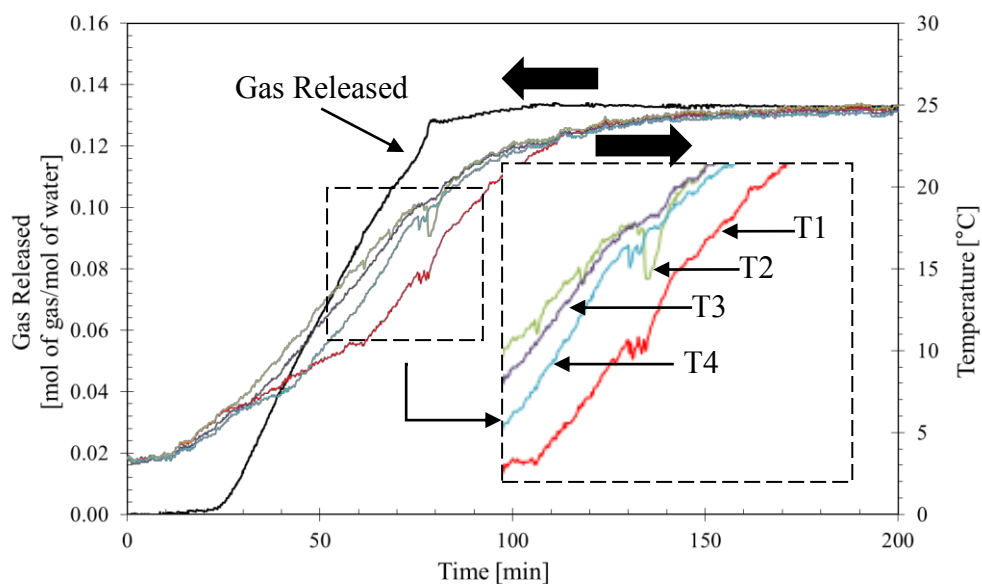


**Figure 4.7** Methane released and temperature profiles in the system of HSC/H<sub>2</sub>O/CH<sub>4</sub> with the 1:12 HSC to water ratio and temperature driving force = 294 K (Experiment 14, Table 4.2).

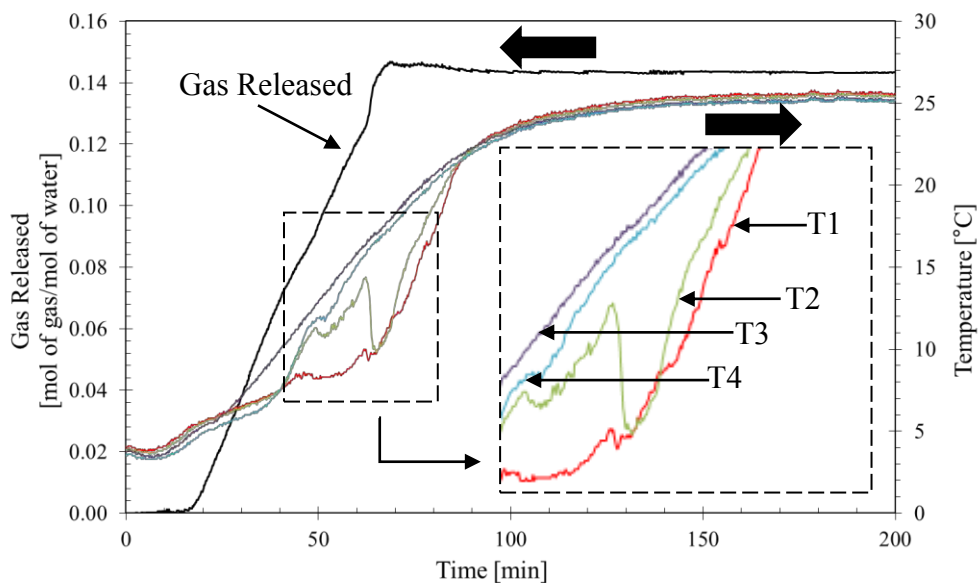


**Figure 4.8** Methane released and temperature profiles in the system of HSC/H<sub>2</sub>O/CH<sub>4</sub> with the 1:14 HSC to water ratio and temperature driving force = 294 K (Experiment 18, Table 4.2).

## 4.2 Effects of Activated Carbon

### 4.2.1 Methane Hydrate Formation

The result of the methane hydrate formation with the presence of activated carbon at 8 MPa and 277 K is shown in Table 4.3. The amount of water was varied so the AC to water ratio is 1:0.8, 1:1, and 1:1.2. The system with the 1:1 AC to water ratio is used as the system saturated with water, which the system with 1:0.8 AC to water ratio has about 20% less water compared with the 1:1 HSC to water ratio case. On the other hand, the 1:1.2 AC to water ratio has 20% more water than the saturated case. The induction times from the three different AC to water ratios are different, meaning that the induction time depends on the amount of water. The results in the table show that the induction time increases with the increase in the water content. The methane consumed and water conversion to hydrates of these systems also change in the same trend. That is they increase with the amount of water. It was reported that, during the hydrate formation, methane is consumed rapidly

because the growth of the hydrate crystals in the interstitial and interconnectivity spaces between the AC particles where the water is located (Siangsai *et al.*, 2015). Hence, the amount of water plays a critical role in the methane consumed and water conversion to hydrates.

Figure 4.9 shows the gas uptake and temperature profiles during the methane hydrate formation of AC/H<sub>2</sub>O/CH<sub>4</sub> system with the 1:0.8 AC to water ratio at 8 MPa and 277 K (Experiment 20, Table 4.3). The formation of hydrates can be observed by the heat released (an exothermic reaction). As seen from the figure, after the methane gas is introduced into the system, the gas can adsorb on the dry carbon surface during the gas dissolution, which can be noticed by the small temperature spike during the first 15 minutes. The general methane hydrate structure includes 46 water molecules and 8 methane molecules, CH<sub>4</sub>·xH<sub>2</sub>O, and x = 5.75 for type I structure. Zhou *et al.*, (2005) reported that if the number of water ratio is smaller than 5.75, there is not enough water for hydrate formation. In this case, the ratio of water to methane is 5.69, which is lower than the number ratio of type I structure, 5.75. Hence, the decrease in the methane gas pressure is possibly due to the methane adsorption on the AC, and the first temperature spike of all thermocouples in the crystallizer could be from the effects of methane adsorption. The second temperature spike is present due to a thin film of hydrates occurs from the nucleation. The methane gas is further consumed continuously until it reaches to the limit of hydrates formation.

The gas uptake and temperature profiles during the methane hydrate formation of the AC/H<sub>2</sub>O/CH<sub>4</sub> system with the 1:1 AC to water ratio (Experiment 22, Table 4.3) is shown in Figure 4.10. It can be observed that the methane gas is dissolved into the liquid phase until it saturates, and hydrate nucleation is formed, which is noticed by the temperature spike in the crystallizer. The thermocouple T1 in the crystallizer located at the top of the crystallizer rises first. Then, the gas uptake rapidly increases because the hydrate growth. Afterwards, the temperature of all thermocouples reach the plateau, meaning that there is no further hydrate formation in the crystallizer.

**Table 4.3** Methane hydrate formation experimental conditions in the system with the presence of activated carbon at 8 MPa and 277 K

EXP. No.	#AC to Water Ratio	Amount of Water Used [ml]	Experimental Pressure [MPa]	Experimental Temperature [°C]	*Induction Time [min]	CH <sub>4</sub> Consumed [mol/mol of H <sub>2</sub> O]	Water Conversion to Hydrate [%mol]
19	1:0.8	8	8	4	1.33	0.0424	54.81
20	1:0.8	8	8	4	1.17	0.0412	53.31
21	1:0.8	8	8	4	0.83	0.0449	58.03
					Average	0.0428±0.0018	55.38±2.41
22	1:1	10	8	4	60.17	0.0588	67.67
23	1:1	10	8	4	52.00	0.0622	67.76
24	1:1	10	8	4	46.17	0.0738	66.38
					Average	0.0649±0.0078	67.27±0.77
25	1:1.2	12	8	4	98.33	0.0803	75.53
26	1:1.2	12	8	4	78.33	0.0775	73.03
27	1:1.2	12	8	4	84.00	0.0789	74.13
					Average	0.0789±0.0014	74.23±1.25

#By weight

\*Induction Time = Time at the first hydrate formation

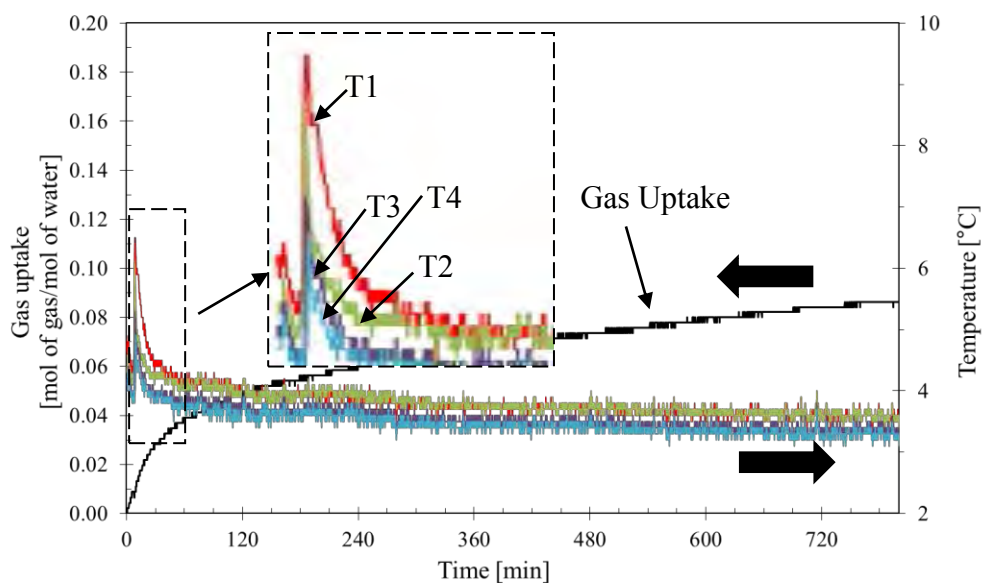


**Figure 4.9** Gas uptake and temperature profiles during the methane hydrate formation of AC/H<sub>2</sub>O/CH<sub>4</sub> system at 8 MPa and 277 K and 1:0.8 AC to water ratio (Experiment 20, Table 4.3).

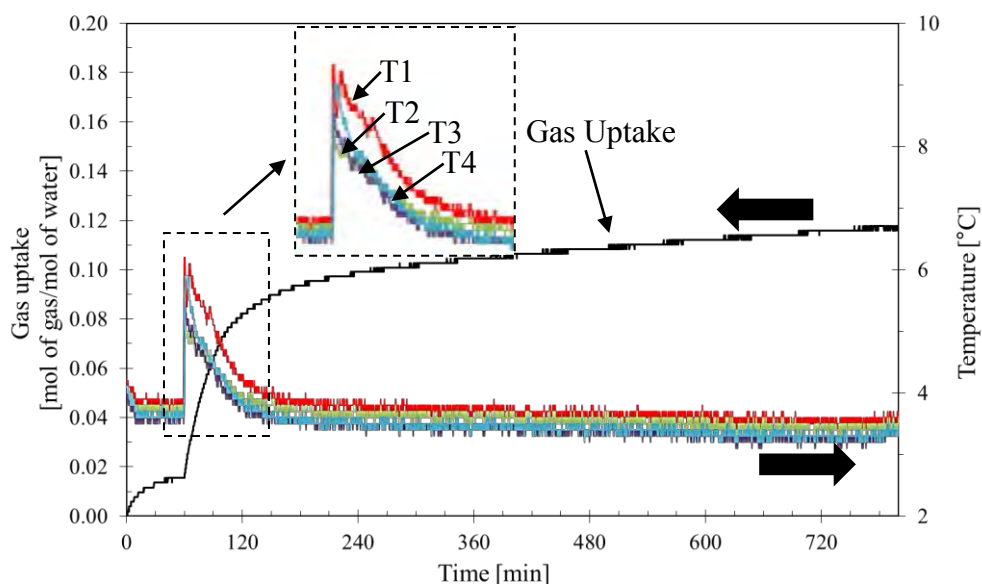


**Figure 4.10** Gas uptake and temperature profiles during the methane hydrate formation of AC/H<sub>2</sub>O/CH<sub>4</sub> system at 8 MPa and 277 K and 1:1 AC to water ratio (Experiment 22, Table 4.3).

The Figure 4.11 shows the gas uptake and temperature profiles during the methane hydrate formation of the AC/H<sub>2</sub>O/CH<sub>4</sub> system with the 1:1.2 AC to water ratio (Experiment 27, Table 4.3). It can be noticed that the methane uptake and temperature profiles is almost the same as the case 1:1 AC to water ratio. At time zero, the temperatures gradually decrease because the gas dissolved into the liquid phase. Subsequently, the water is saturated with the methane gas and the hydrate nucleation formed, which is observed by the rising of the temperatures. After that, the methane is consumed in order to grow the hydrate crystals.

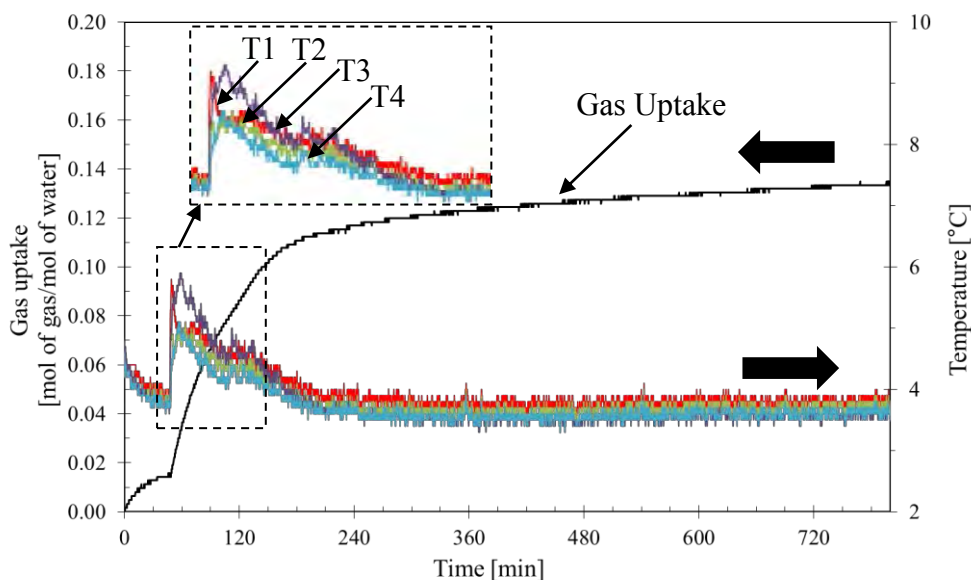


**Figure 4.11** Gas uptake and temperature profiles during the methane hydrate formation of AC/H<sub>2</sub>O/CH<sub>4</sub> system at 8 MPa and 277 K and 1:1.2 AC to water ratio (Experiment 27, Table 4.3).

Figure 4.12 presents the comparison of gas uptake during the methane hydrate formation in the system of AC/H<sub>2</sub>O/CH<sub>4</sub> with the 1:0.8, 1:1, and 1:1.2 AC to water ratios. The system with the 1:0.8 AC to water ratio has the lower initial hydrate formation rate,  $0.0008 \pm 0.0001$  mol/ mol of H<sub>2</sub>O/ second, which can be observed by the slope of the methane uptake profiles, and faster induction time than that with the 1:1 and 1:1.2 AC to water ratios. It could be that the pores of the AC and the interfacial area between the gas and water interface allow the gas to pass through the

carbon bed easily, which promote the hydrate formation (Chari *et al.*, 2013a). The systems with the 1:1 and 1:1.2 AC to water ratios have about the same initial hydrate formation rate,  $0.0012 \pm 0.0001$  and  $0.0011 \pm 0.0002$  mol/ mol of H<sub>2</sub>O/ second. That is because the AC and the high amount of water could increase the contact area between methane gas and water results in a higher initial methane hydrate formation rate than that of the low water content.

Furthermore, the system with the 1:1 and 1:1.2 AC to water ratios have higher water conversion to hydrates than that with the 1:0.8 AC to water ratio. This could be that the 1:1.2 AC to water ratio supplies excess water to fill in the pore, interstitial, and interconnectivity spaces, which then converts to hydrates. Unlike the system with the 1:0.8 AC to water ratio, which has lower amount of water to convert to hydrates. For the system with the 1:1 AC to water ratio, the pores are completely saturated with water, and there may be a small amount of water located at the space between carbon particles, which enhances the contact area more than that the case with the 1:0.8 AC to water ratio. Even though the systems with the 1:1 and 1:1.2 AC to water ratios have sufficient water to convert to hydrates, the system with the 1:1.2 AC to water ratio has higher water conversion to hydrate than that with the 1:1 AC to water ratio. That is due to the system with the 1:1.2 AC to water ratio has water located at the top of the bed, which forms a thin layer above the AC bed, to trigger the nucleation easier and more water than that with the 1:1 AC to water ratio leading to the highest water conversion to hydrates.

The methane consumed from the system with the 1:1.2 AC to water ratio is higher than that with the other two ratios, 1:0.8 and 1:1. This is consistent with the water conversion to hydrates. To form one mole of methane hydrates, 5.75 mole of water are needed. Hence, the system with the 1:1.2 AC to water ratio that has excess water has the highest methane consumed. On the other hand, when the bulk of water is much higher than the AC bed or form in a thick layer, the methane consumed decreases as the result from the thin film layer like hydrates at gas and liquid interface blocking the methane dissolution into water (Govindaraj *et al.*, 2015). Therefore, the volume of water in the system of AC/H<sub>2</sub>O/CH<sub>4</sub> is an important factor for the initial hydrate formation rate, induction time, methane consumed, and water conversion to hydrates.



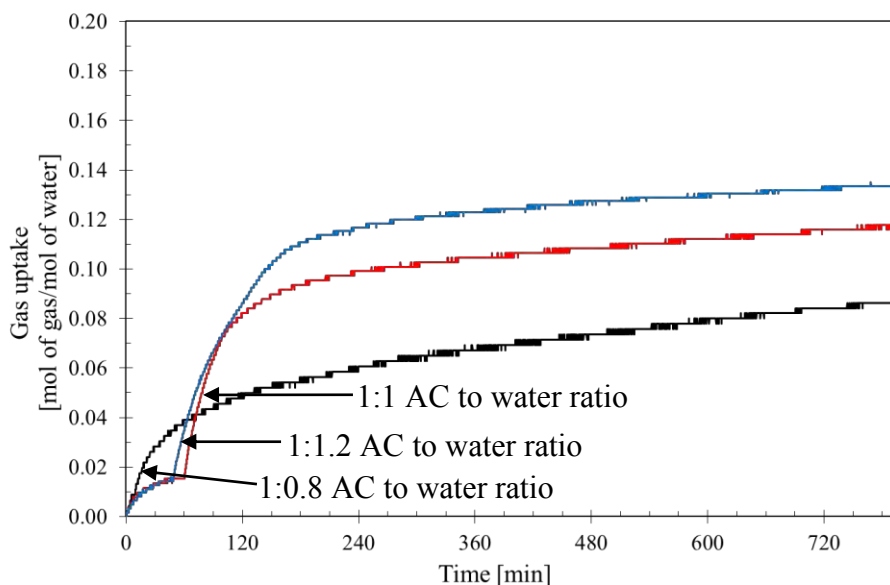


**Figure 4.12** Comparison of hydrate growth during the methane hydrate formation in the system of AC/H<sub>2</sub>O/CH<sub>4</sub> at 8 MPa, 277 K, 1:0.8, 1:1, and 1:1.2 AC to water ratio (Experiments 20, 22, and 27 respectively, Table 4.3). Time zero in the figure corresponds to the first point of hydrate growth.

#### 4.2.2 Methane Hydrate Dissociation

Table 4.4 shows methane hydrate dissociation condition in the systems of AC/H<sub>2</sub>O/CH<sub>4</sub> at 294 K. The systems with the 1:0.8, 1:1, and 1:1.2 AC to water ratios have the same dissociation temperature ( $T_d$ ), which is the first temperature that the methane is released from the hydrate crystals, and the same final methane recovery as the HSC/H<sub>2</sub>O/CH<sub>4</sub> cases. From the table, the methane released seems to vary with the AC: water ratio. However, the amount of methane released depends on the methane consumed in each system. Hence, the methane recovery is used for the comparison purpose. Thus, increasing the amount of water does not affect the methane released and methane recovery at the same temperature driving force (294 K).

Figures 4.13 and 4.14 present methane released and temperature profiles in the systems of AC/H<sub>2</sub>O/CH<sub>4</sub> with the 1:0.8 and 1:1 AC to water ratios, respectively, at 294 K temperature driving force. As seen from the figures, the temperature in the crystallizer gradually increases by the thermal stimulation. Once the temperature in the crystallizer crosses the equilibrium point, the methane starts to release from the hydrates as indicated by the temperature drop in the profiles. The thermocouple T1 located at the top of the bed indicates that the dissociation at the gas and liquid interface is the slowest due to the stability of the hydrates at this location. After the methane hydrate decomposition completes, the temperature in the crystallizer gradually increases until it reaches the plateau at 298 K.

The methane released and temperature profiles in the system with the 1:1.2 AC to water ratio is shown in Figure 4.15. It can be noticed that the methane released and temperature profiles are quite similar to the other two systems but the temperature of thermocouple T3 takes the longest time for dissociation, meaning that the methane hydrates at that T3 location, which is located at the middle of the carbon bed, is more stable than the other locations. Hence, varying the AC to water ratio does not affect the final methane recovery.

**Table 4.4** Methane hydrate dissociation experimental conditions in the system with the presence of activated carbon using  $^a\Delta T = 294$  K

EXP. No.	AC to Water Ratio	$\Delta T_a$ [°C]	Dissociation Temperature, $T_d^b$ [°C]	CH <sub>4</sub> Released [mol/mol of H <sub>2</sub> O]	CH <sub>4</sub> Recovery [mol%]
28	1:0.8	21	7.5	0.0401	94.50
29	1:0.8	21	7.6	0.0383	92.88
30	1:0.8	21	7.5	0.0411	91.53
			Average	0.0398±0.0014	92.97±1.48
31	1:1	21	7.2	0.0577	98.12
32	1:1	21	7.0	0.0611	98.23
33	1:1	21	7.2	0.0731	99.05
			Average	0.0640±0.0081	98.47±0.51
34	1:1.2	21	7.2	0.0725	90.29
35	1:1.2	21	7.1	0.0697	89.94
36	1:1.2	21	7.2	0.0711	90.11
			Average	0.0711±0.0014	90.11±0.17

$^a\Delta T = T_{\text{end}} - T_{\text{start}}$

$^bT_d$  = Dissociation temperature

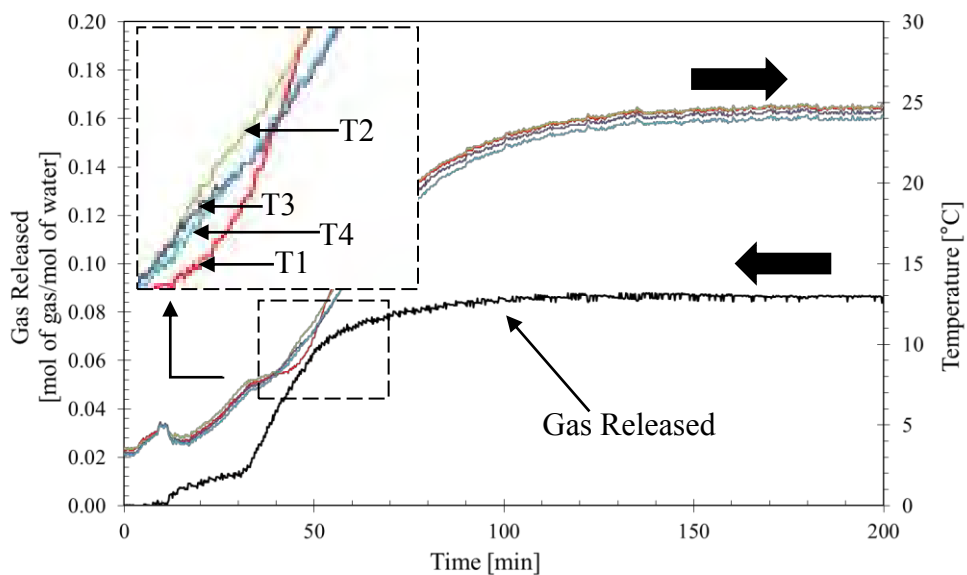


**Figure 4.13** Methane released and temperature profiles in the system of AC/H<sub>2</sub>O/CH<sub>4</sub> at 1:0.8 AC to water ratio and temperature driving force = 294 K (Experiment 29, Table 4.4).

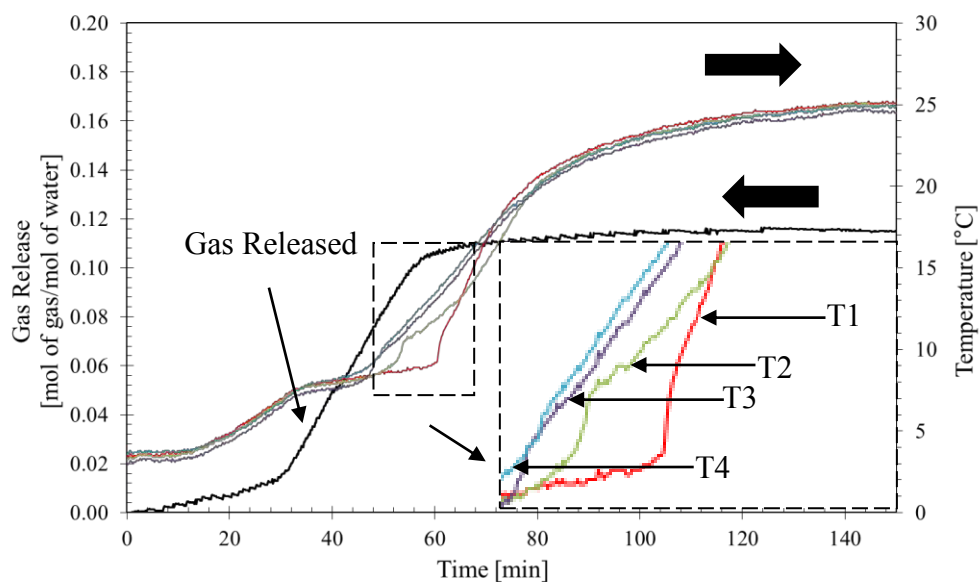


**Figure 4.14** Methane released and temperature profiles in the system of AC/H<sub>2</sub>O/CH<sub>4</sub> at 1:1 AC to water ratio and temperature driving force = 294 K (Experiment 31, Table 4.4).

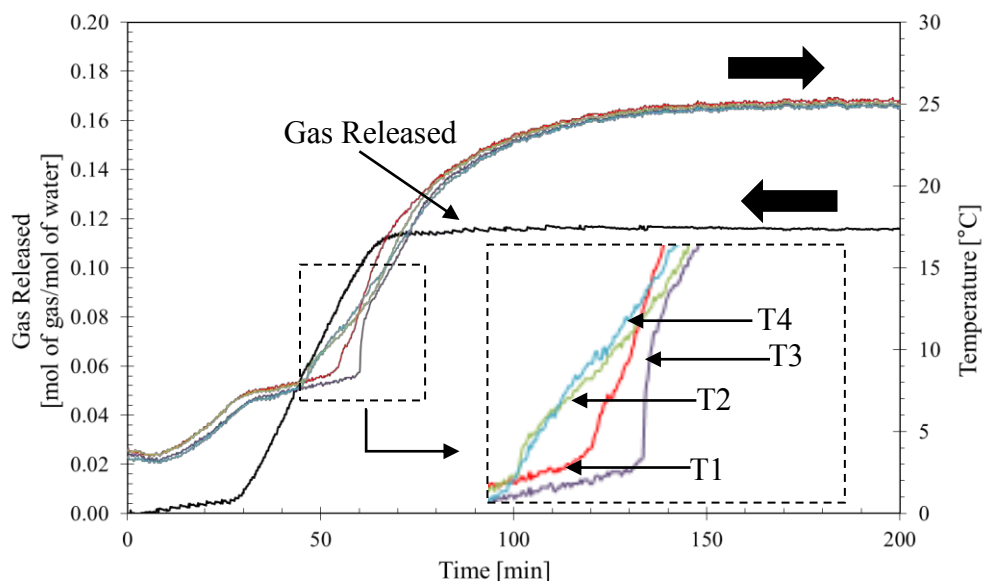


**Figure 4.15** Methane released and temperature profiles in the system of AC/H<sub>2</sub>O/CH<sub>4</sub> at 1:1.2 AC to water ratio and temperature driving force = 294 K (Experiment 36, Table 4.4).

### 4.3 Comparison between the Effects of Hollow Silica and Activated Carbon to Water Ratio

Comparison between the effects of HSC and AC will be made. It will be separated into these cases depending on the amount of water involved in the system. The results from Figures 4.16, 4.17, and 4.18 indicate that all the systems with the presence of HSC have higher methane consumed than the systems with the presence of AC because of the nature of the HSC structure. This structure has a hollow core surrounded by a thin solid shell and could be cracked resulting in the presence of the multiple nucleation, which increases the water conversion to hydrates and methane consumed.

The comparison of gas uptake in the case of water deficit, 1:10 HSC to water ratio and 1:0.8 AC to water ratio, is shown in Figure 4.16. The porous bed has both wet and dry materials in the crystallizer. As AC is a hydrophilic and microporous material, the capillary effect caused by AC small pores results in the

lower amount of water coated on the AC surface than the HSC (Liu and Flemings, 2011). In contrast, the HSC, a hydrophobic material with its particle size and interstitial space in the bed relatively smaller than the AC, could promote the movement of water by capillary action along with the wet HSC. This could be the reason that the HSC has a high contact area between gas and liquid phase (Veluswamy *et al.*, 2016). Therefore, the amount of water covers the wet AC is lower than that of the wet HSC. The low amount of water at the interstitial and interconnectivity spaces of the AC results in the low methane consumed. For the system with the HSC, the hydrates formed at the interface could be cracked and induce methane hydrate formation again corresponding to the multiple nucleation, which facilitates the high methane consumed (Jin *et al.*, 2012).

Furthermore, the comparison of gas uptake of the porous materials saturated with water, 1:12 HSC to water ratio and 1:1 AC to water ratio, is presented in Figure 4.17. The HSC and AC are wetted and have some water at the gap between particles. The HSC particle size is smaller than the AC, 30-70  $\mu\text{m}$  and 420-841  $\mu\text{m}$ , respectively, leading to larger contact area between gas and liquid phase than the system with the AC. That, in turn, results in the higher amount of water at the interstitial and interconnectivity spaces than the system with the AC system, leading to the high water conversion to hydrates and high methane consumed.

The comparison of gas uptake of the excess water system, 1:14 HSC to water ratio and 1:1.2 AC to water ratio, is shown in Figure 4.18. Because of its low density, the HSC is float on the water surface. From the experiment, it was observed that the floating HSC particles are wet. This increases the contact between the methane gas and water. Consequently, the system with the 1:14 HSC to water ratio has higher methane consumed than that with the 1:1.2 AC to water ratio. In contrast, the excess water in the system with the AC has the bed covered by a water layer, which could block the gas dissolved into the water. Therefore, the nature of the HSC and the amount of water can enhance the methane consumed efficiently more than the AC on the methane hydrate formation.

For the induction time, it can be clearly seen that all systems with the presence of HSC has a longer induction time than that those with the AC. That is because a large surface area and high tendency to adsorb methane of the AC supplementing the solubility, which facilitates the nucleation (Govindaraj *et al.*, 2015).

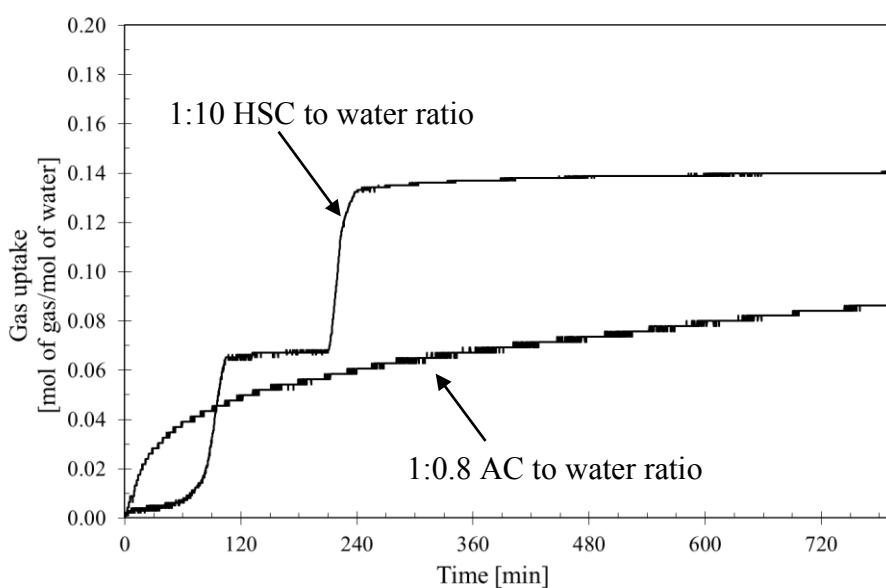


**Figure 4.16** Comparison of gas uptake during the methane hydrate formation in the system of water deficit (1:10 HSC to water ratio and 1:0.8 AC to water ratio) with the present of HSC and AC at 8 MPa and 277 K.

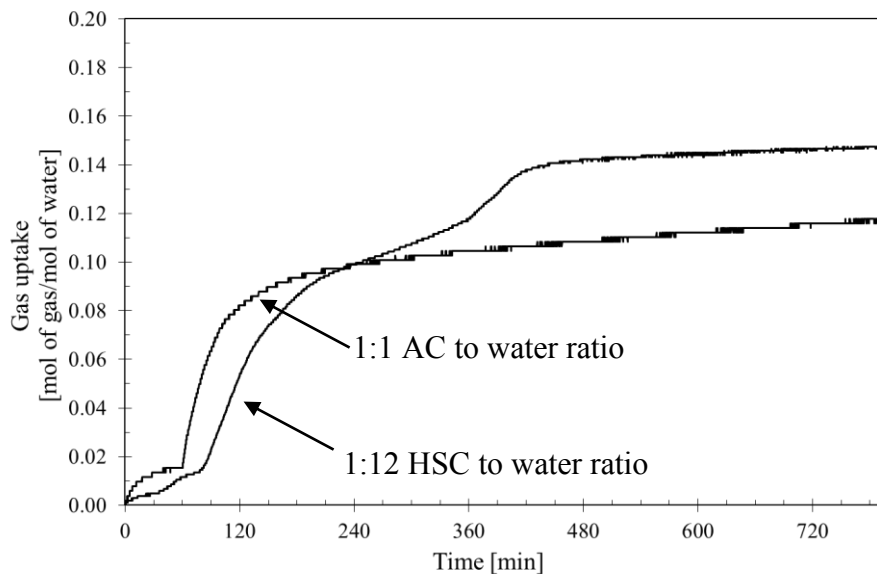


**Figure 4.17** Comparison of gas uptake during the methane hydrate formation in the system of water saturated (1:12 HSC to water ratio and 1:1 AC to water ratio) with the present of HSC and AC at 8 MPa and 277 K.

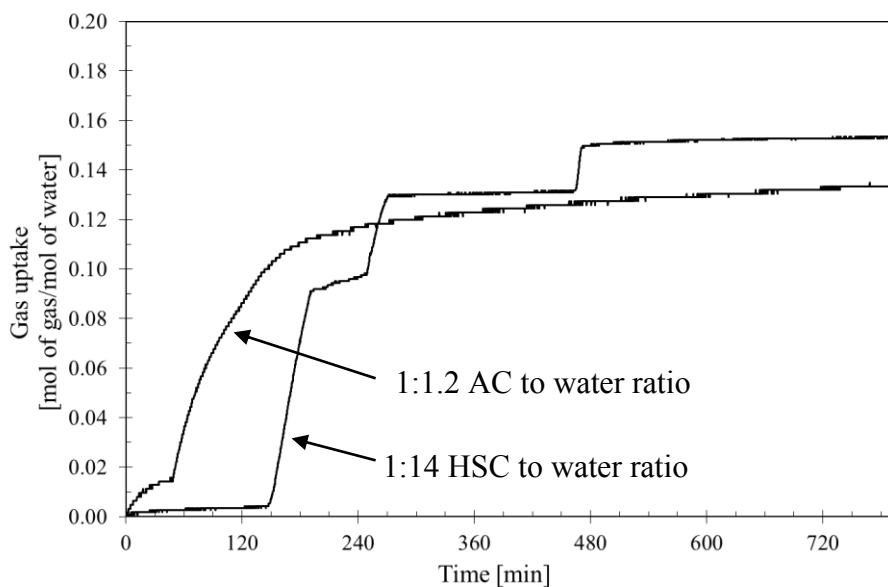


**Figure 4.18** Comparison of gas uptake during the methane hydrate formation in the system of excess water (1:14 HSC to water ratio and 1:1.2 AC to water ratio) with the present of HSC and AC at 8 MPa and 277 K.



## **CHAPTER V**

### **CONCLUIONS AND RECOMMENDATIONS**

#### **5.1 Conclusions**

Methane hydrate formation and dissociation with the presence of hollow silica and activated carbon were conducted to study the effects of the porous materials and the porous materials to water ratios. It was observed that the presence of the porous materials affect the induction time of the hydrate formation and methane consumed. The low density and small particle sizes of hollow silica may aid the high methane consumption due to the high interconnectivity and interstitial spaces, which increase the contact area between gas and liquid phases. The solubility of gas is improved by the large surface area and the tendency to adsorb methane of the AC. That is the reason for the fast induction time of the system with the AC. Moreover, the quantity of water in the system with the presence of porous materials also affects both induction time and methane consumed. The results from the HSC system with saturated water shows that the water conversion to hydrates and methane consumed are higher than the AC system with saturated water due to the hydrophobicity of HSC has more water at the interconnectivity and interstitial spaces between particles. However, the HSC system has longer induction time than that the AC system because the AC has a larger surface area than the HSC. Decreasing water about 20% less from the saturated water system results in the low water conversion to hydrates and methane consumed because the insufficient water to convert to hydrates. The AC system with water deficit can enhance the fast induction time because it allows the gas to pass through the dry porous bed easily. Increasing water about 20% more from the saturated water system results in the high water conversion to hydrates and methane consumed. The induction time also increases due to the increase in the mass transfer resistance of water, which could inhibit the gas dissolved into the water.

For the methane hydrate dissociation, the final methane recovery in the system of different HSC or AC to water ratios are not significantly different at the same temperature driving force (294 K). The type of porous materials and amount of

water do affect the induction time and methane consumed but not the methane hydrate dissociation.

## **5.2 Recommendations**

The following recommendations for research are based on the study findings:

1. Use the activated carbon with the same size as hollow silica (30-70  $\mu\text{m}$ ) to investigate the hydrate formation and dissociation.
2. Coating activated carbon with silane coupling agents to enhance the methane consumed in the methane hydrate formation.

## REFERENCES

- Asheh, S., and Edami, K. (2008) Sorptive storage of natural gas on molecular sieves: Dynamic Investigation. World Academy of Science, 2, 158-165.
- Babakhani, S.M., and Alamdari, A. (2015) Effect of maize starch on methane hydrate formation/dissociation rates and stability. Journal of Natural Gas Science and Engineering, 26(8), 1-5.
- Babu, P., Kumar, R., and Linga, P. (2013) Pre-combustion capture of carbon dioxide in a fixed bed reactor using the clathrate hydrate process. Energy, 50, 364-373.
- Babu, P., Kumar, R., and Linga, P. (2014) Unusual behavior of propane as a co-guest during hydrate formation in silica sand: Potential application to seawater desalination and carbon dioxide capture. Chemical Engineering Science, 117, 342–351.
- Ballard, A. L., and Sloan, E. D. (2000) Structural transitions in methane+ethane gas hydrates, Part II: Modeling beyond incipient conditions. Chemical Engineering Science, 55, 5773-5782.
- Celzard, A., and Mareche, J.F. (2005) Optimal wetting of active carbons for methane hydrate formation. Fuel, 85, 957–966.
- Chari, V.D., Raju, B., Prasad, P.S.R., and Rao, D.N. (2013a) Methane hydrates in spherical silica matrix: Optimization of capillary water. Energy and Fuels, 27, 3679-3984.
- Chari, V.D., Sharma, D.V.S.G.K., Prasad, P.S.R., and Murthy, S.R. (2013b) Methane hydrates formation and dissociation in nano silica suspension. Journal of Natural Gas Science and Engineering, 11, 7-11.
- Chari, V.D., Prasad, P.S.R., and Murthy, S.R. (2015) A novel material for methane storage. Oil and Gas Science and Technology, 70, 1125-1132.
- Chong, Z.R., Chan, A.H.M., Babu, P., Yang, M., and Linga, P. (2015) Effect of NaCl on methane hydrate formation and dissociation in porous media. Journal of Natural Gas Science and Engineering, 27, 178-189.

- Englezos, P., and Lee, J.D. (2005) A cleaner source of energy and opportunity for innovative technologies. Department of Chemical & Biological Engineering, The University of British Columbia, 22(5), 671-681.
- Gabbito, J.F., and Tsouris, C. (2009). Physical properties of gas hydrates. Journal of Thermodynamics, 271-291.
- Govidaraj, V., Mech, D., Pandey, G., Nagarajan, R., and Sangwai, J.S. (2015) Kinetics of methane hydrate formation in the presence of activated carbon and nano-silica suspensions in pure water. Journal of Natural Gas Science and Engineering, 26, 810-818.
- Henriet, J.P., and Mienert, J. (1998) Gas hydrates relevance to world margin stability and climate change. London: The Geological Society.
- Javanmardi, J., Nasrifar, KH., Najibi, S.H., and Moshfeghian, M. (2005) Economic evaluation of natural gas hydrate as an alternative for natural gas transportation. Applied Thermal Engineering, 25, 1708–1723.
- Jin, K., Konno, Y., and Nagao, J. (2012) Growth of Methane Clathrate Hydrates in Porous Media. Energy and Fuels, 26, 2242-2247.
- Kumar, A., Bhattacharjee, G., Kulkarni, B. D., and Kumar, R. (2015) Role of surfactants in promoting gas hydrate formation. Industrial and Engineering Chemistry Research, 54, 12217–12232.
- Khurana, M., Yin, Z., and Linga, P. (2017) A review of clathrate hydrate nucleation. American Chemical Society, 5, 11176-11203.
- Linga, P., Haligva, C., Nam, S.C., Ripmeester, J.A., and Englezos, P. (2009) Gas hydrate formation in a variable volume bed of silica sand particles. Energy and Fuels, 23, 5496–5507.
- Liu, X., and Femings, F.B. (2011) Capillary effects on hydrate stability in marine sediments. Journal of Geophysical Research, 116, 7102-7126.
- Mekala, P., Babu, P., Sangwai, J.S., and Linga, P. (2014) Formation and dissociation kinetics of methane hydrates in seawater and silica sand. Energy and Fuels, 28, 2708–2716.

- Prasad, P.S. R., Sowjanya, Y., and Chari, V.D. (2014) Enhancement in methane storage capacity in gas hydrates formed in hollow silica. The Journal of Physical Chemistry C, 118, 7759–7764.
- Prasad, P.S.R. (2015) Methane hydrate formation and dissociation in the presence of hollow silica. Journal of Chemical and Engineering Data, 60, 304-310.
- Rodger, P.M. (1989) Stability of gas hydrates. The Journal of Physical Chemistry, 94, 6080-6089.
- Seo, Y., Shin, K., Kim, H., Wood, C.D., Tian, W., and Kozielski, A.K. (2014) Preventing gas hydrate agglomeration with polymer hydrogels. Energy and Fuels, 4409-4420.
- Siangsai, A., Rangsunvigit, P., Kitiyanan, B., Kulprathipanja, S., and Linga, P. (2015) Investigation on the roles of activated carbon particle sizes on methane hydrate formation and dissociation. Chemical Engineering Science, 126, 383–389.
- Sloan, E.D. (1997) Gas hydrates: Review of physical/chemical properties. Energy and fuels, 12, 191-196.
- Sloan, E.D. (2003) Fundamental principles and applications of natural gas hydrates. Nature Publishing Group, 426.
- Sloan, E.D., and Koh, C.A. (2007) Clathrate hydrates of natural gases, Third edition. California: CRC press.
- Suesuan, R. (2015) Comparative study on the effects of hollow silica and activated carbon on methane hydrate formation and dissociation. Chulalongkorn University, Bangkok, Thailand.
- Sun, Z.G., Ma, R., Wang, R.Z., Guo, K.H., and Fa, S.S. (2003) Experimental studying of additives effects on gas storage in hydrates. Energy and Fuels, 17, 1180-1185.
- Sun, Z., Ma, R., Fan, S., Guo, K., and Wang, R. (2004) Investigation on gas storage in methane hydrate. Journal of Natural Gas Chemistry, 13, 107– 112.
- Thomas, S., and Dawe, R.A. (2003) Review of ways to transport natural gas energy from countries which do not need the gas for domestic use. Energy, 28, 1461–1477.

- Veluswamy, H.P., Prasad, P.S.R., and Linga, P. (2015) Mechanism of methane hydrate formation in the presence of hollow silica. Korean Journal Chemical Engineering Journal, 33(7), 2050-2062.
- Veluswamy, H.P., Wong, A.J.H., Babu, P., Kumar, R., Kulprathipanja, S., Rangsunvigit, P., and Linga, P. (2016) Rapid methane hydrate formation to develop a cost effective large scale energy storage system. Chemical Engineering Journal, 290, 161-173.
- Zhang, Y., Li, X., Chen, Z., Li, G., and Wang, Y. (2016) Effects of particle and pore sizes on the formation behaviors of methane hydrate in porous silica gels. Journal of Natural Gas Science and Engineering, 35, 1463-1471.
- Zhenyuan, Y., Chong, Z.R., Tan, H.K., and Linga, P. (2016) Review of gas hydrate dissociation kinetic models for energy recovery. Journal of Natural Gas Science and Engineering, 35, 1362-1387.
- Zhou, Y., Wang, Y., Chen, H., and Zhou, L. (2005) Methane storage in wet activated carbon: Studies on the charging/discharging process. Carbon, 43, 2007-2012.
- Bignell, C. "LNG: what is boil-off gas and what does it do" fluenta. 8 January 2018. 12 January 2018 <<https://www.fluenta.com/news/lng-boil-off-gas/>>
- Kate, M. "How Do Fossil Fuels Form" Socratic. 20 March 2016. 7 July 2017 <<https://socratic.org/questions/how-do-fossil-fuels-form>>
- King, H.M. "Methane hydrate" Geology. 7 July 2017 <<https://geology.com/articles/methane-hydrates/>>
- Plumer, B. "Are methane hydrates the next big energy source." Washingtonpost. 12 March 2013. 7 July 2017 <[https://www.washingtonpost.com/news/wonk/wp/2013/03/12/japan-tries-to-unlock-the-worlds-biggest-source-of-carbon-based-fuel/?utm\\_term=.b88e0bcd2c05](https://www.washingtonpost.com/news/wonk/wp/2013/03/12/japan-tries-to-unlock-the-worlds-biggest-source-of-carbon-based-fuel/?utm_term=.b88e0bcd2c05)>
- Woodrow, L. "Japan Extracts Natural Gas from Frozen Methane." 14 March 2013. 6 July 2017 <<http://www.theenergycollective.com/lee-woodrow/197921/extracted-natural-gas-frozen-methane-hydrate>>

## APPENDICES

### Appendix A Calculation for the Methane Consumption

$$\text{From; } \Delta n_{H,\downarrow} = n_{H,t} - n_{H,0} = \left(\frac{PV}{zRT}\right)_{G,0} - \left(\frac{PV}{zRT}\right)_{G,t}$$

where  $\Delta n_{H,\downarrow}$  = moles of consumed gas for hydrate formation (mole)

$\Delta n_{H,t}$  = moles of hydrate at time t, (mole)

$\Delta n_{H,0}$  = moles of hydrate at time 0, (mole)

P = pressure of the crystallizer, (atm)

T = temperature of the crystallizer, (K)

V = the volume of gas phase in the crystallizer, (cm<sup>3</sup>)

Z = compressibility factor

R = the universal gas constant 82.06 cm<sup>3</sup> atm/mol K

#### Properties of methane

Critical Temperature (T<sub>c</sub>) = 190.45 K

Critical Pressure (P<sub>c</sub>) = 4596 kPa

Acentric Factor (ω) = 0.00115

**Step 1:** To find pressure reduced (Pr) and temperature reduced (Tr)

Data: Experimental number 1

At time 0, Pressure (P) = 8000 kpa = 78.95 atm

Temperature (K) = 277 K

At time t, Pressure (P) = 7057 kpa = 69.65 atm

Temperature (K) = 277 K

Solution;  $T_r = \frac{T}{T_c} = \frac{277 \text{ K}}{190.45 \text{ K}} = 1.45$

$$\text{At time } 0, \quad P_r = \frac{P}{P_c} = \frac{8000 \text{ kpa}}{4596 \text{ kpa}} = 1.74$$

$$\text{At time } t, \quad P_r = \frac{P}{P_c} = \frac{7057 \text{ kpa}}{4596 \text{ kpa}} = 1.54$$

**Step 2:** To find volume of adsorbent ( $V_{\text{ads}}$ ) and volume of gas phase ( $V_{\text{cr}}$ ) Data:

Volume of reactor with reservoir ( $V_{\text{reactor}}$ ) = 146.94 cm<sup>3</sup>

Use activated carbon 9.0537 g

Weight of adsorbent ( $W_{\text{ads}}$ ) = 9.0537 g

$$V_{\text{ads}} = \frac{\text{Weight}_{\text{ads}}}{\text{Density}_{\text{ads}}} = \frac{9.0537}{0.4426} = 22.4557 \text{ cm}^3$$

$$\text{Volume of gas phase} = V_{\text{reactor}} - V_{\text{ads}} = 146.94 - 22.46 = 124.48 \text{ cm}^3$$

**Step 3:** To find compressibility factor ( $z$ )

$$\beta^0 = \frac{0.083 - 0.422}{T_r^{1.6}} = \frac{0.083 - 0.422}{1.45^{1.6}} = -0.19$$

$$\beta^1 = \frac{0.139 - 0.172}{T_r^{4.2}} = \frac{0.139 - 0.172}{1.45^{4.2}} = -6.9 \times 10^3$$

Time 0;

$$z = 1 + \beta^0 \frac{P_r}{T_r} + \omega \beta^1 \frac{P_r}{T_r} = 1 + (-0.19) \left( \frac{1.74}{1.45} \right) + (0.00115) (-6.9 \times 10^3) \left( \frac{1.74}{1.45} \right) = 0.77$$

Time 0;

$$z = 1 + \beta^0 \frac{P_r}{T_r} + \omega \beta^1 \frac{P_r}{T_r} = 1 + (-0.19) \left( \frac{1.54}{1.45} \right) + (0.00115) (-6.9 \times 10^3) \left( \frac{1.54}{1.45} \right) = 0.79$$

**Step 4:** To find the methane consumption

$$\Delta n_{\text{H},\downarrow} = n_{\text{H},t} - n_{\text{H},0} = \left( \frac{PV}{zRT} \right)_{\text{G},0} - \left( \frac{PV}{zRT} \right)_{\text{G},t}$$



$$= \left( \frac{78.95 \text{ atm} \times 124.48 \text{ cm}^3}{0.77 \times 82.06 \text{ cm}^3 \cdot \frac{\text{atm}}{\text{mol}} \cdot \text{K} \times 277\text{K}} \right)_{G,0} - \left( \frac{69.65 \text{ atm} \times 124.48 \text{ cm}^3}{0.79 \times 82.06 \text{ cm}^3 \cdot \frac{\text{atm}}{\text{mol}} \cdot \text{K} \times 277\text{K}} \right)_{G,t}$$

$$= 0.5615 - 0.4828 = 0.0786$$

So, the methane consumption = 0.0786 mol

The calculation for the methane released has similar step with the methane consumption, but the equation is calculated by

$$\Delta n_{H,\uparrow} = n_{H,0} - n_{H,t} = \left( \frac{PV}{zRT} \right)_{G,t} - \left( \frac{PV}{zRT} \right)_{G,0}$$

where  $\Delta n_{H,\uparrow}$  = moles of released gas from the hydrate

$\Delta n_{H,t}$  = moles of hydrate at time t, (mole)

$\Delta n_{H,0}$  = moles of hydrate at time 0, (mole)

P = pressure of the crystallizer, (atm)

T = temperature of the crystallizer, (K)

V = the volume of gas phase in the crystallizer, (cm<sup>3</sup>)

Z = compressibility factor

R = the universal gas constant 82.06 cm<sup>3</sup> atm/mol K

### Appendix B Calculation for the Conversion of Water to Hydrate

From;

$$\text{Conversion of water hydrates (\%)} = \frac{\Delta n_{H,\downarrow} \times \text{hydration number}}{n_{H_2O}} \times 100$$

where  $n_{H_2O}$  = moles of water in the system, mol

$\Delta n_{H,\downarrow}$  = moles of consumed gas for hydrate formation, mol

Data:

Hydration number of activated carbon = 6.1

$n_{H_2O}$  = Weight water/ Molecular weight water = 10.9 g /18 M.W. = 0.64 mol

$\Delta n_{H,\downarrow}$  = 0.0786 mol

Thus,

$$\text{Conversion of water hydrates (\%)} = \frac{0.0786 \times 6.1}{0.64} \times 100 = 74.91\%$$

### Appendix C Calculation for the Percentage of Methane Recovery

From;

$$\% \text{methane recovery} = \frac{(\Delta n_{H,\uparrow})_t}{(\Delta n_{H,\downarrow})_{end}} \times 100$$

where  $(\Delta n_{H,\uparrow})_t$  = moles of released gas from hydrate during the hydrate dissociation at any given time

$(\Delta n_{H,\downarrow})$  = moles of gas consumption for hydrate formation at the end of experiments.

Data:  $(\Delta n_{H,\uparrow})_t = 0.0711 \text{ mol}$

$(\Delta n_{H,\downarrow}) = 0.0786 \text{ mol}$

Thus,  $\% \text{methane recovery} = \frac{0.0711}{0.0786} \times 100 = 90.11\%$

## Appendix D Reused Hollow Silica

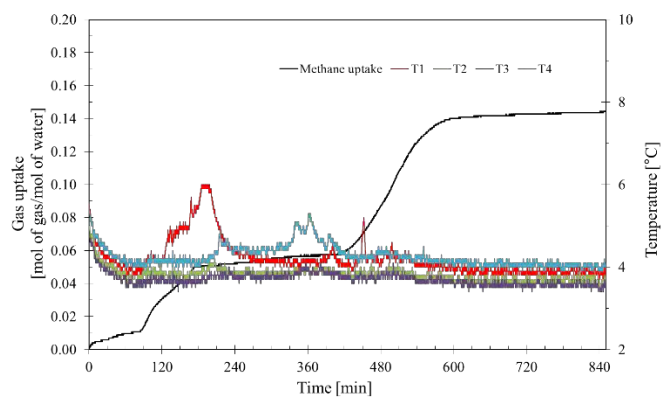


**Figure S1** Gas uptake and temperature profiles during the methane hydrate formation of the HSC/H<sub>2</sub>O/CH<sub>4</sub> system at 8 MPa and 277 K (Fresh HSC).

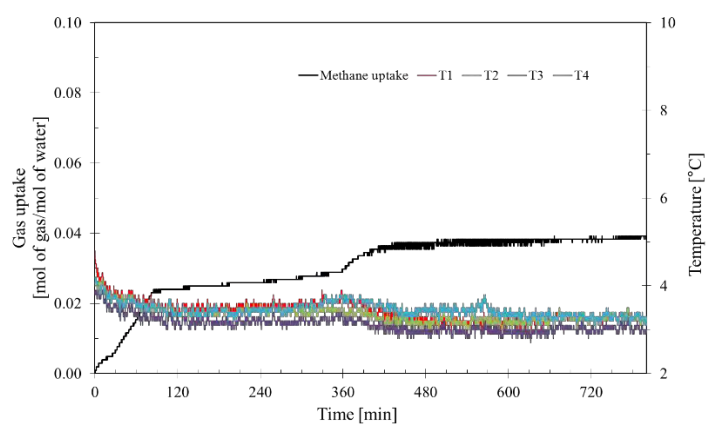


**Figure S2** Gas uptake and temperature profiles during the methane hydrate formation of the HSC/H<sub>2</sub>O/CH<sub>4</sub> system at 8 MPa and 277 K (Reused HSC).

**Table S1** Methane hydrate formation experimental conditions in the system with the presence of hollow silica

HSC	Experimental Pressure [MPa]	Experimental Temperature [°C]	Induction Time [min]	CH <sub>4</sub> Consumed [mol/mol of H <sub>2</sub> O]	Water Conversion to Hydrates [%mol]
Fresh	8	4	82.17	0.1401	80.56
Reused	8	4	17.83	0.0882	50.73

## CURRICULUM VITAE

**Name:** Ms. Sarocha Rungrussamee

**Date of Birth:** July 06, 1993

**Nationality:** Thai

**University Education:**

2012–2016 Bachelor of Science, Industrial Chemistry, King Mongkut's  
Institute of Technology Ladkrabang, Bangkok, Thailand

**Work Experience:**

2015-2015 Position: Quality Control  
Company name: PTT Public Company Limited

**Presentations:**

1. Rungrussamee, S., Kulprathipanja, S., and Rangsunvigit, P. (2018, August 25-29) Comparative Study of Methane Hydrate Formation and Dissociation with Hollow Silica and Activated Carbon. Paper presented at 21<sup>st</sup> Conference on Process Integration, Modelling and Optimisation, Prague, Czech Republic.
2. Rungrussamee, S., Kulprathipanja, S., and Rangsunvigit, P. (2018, May) The Effect of Water on Methane Hydrate Formation and Dissociation with Hollow Silica and Activated Carbon. Paper presented at The 6<sup>th</sup> Research Symposium on Petroleum, Petrochemicals and Advanced Materials and The 21<sup>st</sup> PPC Symposium on Petroleum, Petrochemicals, and Polymers, Bangkok, Thailand.